

# The Surface Atmosphere Integrated Field Laboratory (SAIL) Campaign

D.R. Feldman<sup>1\*</sup>, A.C. Aiken<sup>2</sup>, W. R. Boos<sup>1,3</sup>, R.W.H. Carroll<sup>4</sup>, V. Chandrasekar<sup>5</sup>, S. Collis<sup>6</sup>, J. M. Creamean<sup>5</sup>, G. de Boer<sup>7,8,9</sup>, J. Deems<sup>10</sup>, P. J. DeMott<sup>5</sup>, J. Fan<sup>11</sup>, A. N. Flores<sup>12</sup>, D. Gochis<sup>13</sup>, M. Grover<sup>6</sup>, T. C. J. Hill<sup>5</sup>, A. Hodshire<sup>14</sup>, E. Hulm<sup>15</sup>, C. C. Hume<sup>5</sup>, R. Jackson<sup>6</sup>, F. Junyent<sup>5</sup>, A. Kennedy<sup>16</sup>, M. Kumjian<sup>17</sup>, E. J. T. Levin<sup>14</sup>, J. D. Lundquist<sup>18</sup>, J. O'Brien<sup>6</sup>, M. S. Raleigh<sup>19</sup>, J. Reithel<sup>15</sup>, A. Rhoades<sup>1</sup>, K. Rittger<sup>20</sup>, W. Rudisill<sup>1</sup>, Z. Sherman<sup>6</sup>, E. Siirila-Woodburn<sup>1</sup>, S. M. Skiles<sup>21</sup>, J. N. Smith<sup>22</sup>, R. C. Sullivan<sup>6</sup>, A. Theisen<sup>6</sup>, M. Tuftedal<sup>6</sup>, A. C. Varble<sup>11</sup>, A. Wiedlea<sup>1</sup>, S. Wielandt<sup>1</sup>, K. Williams<sup>1</sup>, Z. Xu<sup>1</sup>



1. Earth and Environmental Sciences Area, Lawrence Berkeley National Laboratory, Berkeley, CA
2. Earth and Environmental Sciences Division, Los Alamos National Laboratory, Los Alamos, NM
3. Department of Earth and Planetary Science, University of California-Berkeley, Berkeley, CA
4. Division of Hydrologic Sciences, Desert Research Institute, Reno, NV
5. Colorado State University, Fort Collins, CO
6. Environmental Science Division, Argonne National Laboratory, Lemont, IL
7. Cooperative Institute for Research in Environmental Sciences, University of Colorado Boulder, Boulder CO
8. NOAA Physical Sciences Laboratory, Boulder, CO
9. Integrated Remote and In Situ Sensing, University of Colorado Boulder, Boulder, CO
10. National Snow and Ice Data Center, University of Colorado Boulder, Boulder, CO
11. Pacific Northwest National Laboratory, Richland, WA
12. Department of Geosciences, Boise State University, Boise, ID
13. National Center for Atmospheric Research, Boulder, CO
14. Handix Scientific, LLC, Fort Collins, CO
15. Rocky Mountain Biological Laboratory, Crested Butte, CO
16. Department of Atmospheric Sciences, University of North Dakota, Grand Forks, ND
17. The Pennsylvania State University, University Park, PA
18. Department of Civil and Environmental Engineering, University of Washington, Seattle WA
19. College of Earth, Ocean, and Atmospheric Sciences, Oregon State University, Corvallis, OR
20. Institute of Arctic and Alpine Research, University of Colorado, Boulder, CO
21. University of Utah, Salt Lake City, UT
22. Department of Chemistry, University of California, Irvine CA

\* Corresponding Author, [drfeldman@lbl.gov](mailto:drfeldman@lbl.gov)

1

**Early Online Release:** This preliminary version has been accepted for publication in *Bulletin of the American Meteorological Society*, may be fully cited, and has been assigned DOI 10.1175/BAMS-D-22-0049.1. The final typeset copyedited article will replace the EOR at the above DOI when it is published.

© 2023 American Meteorological Society. This is an Author Accepted Manuscript distributed under the terms of the default AMS reuse license. For information regarding reuse and general copyright information, consult the AMS Copyright Policy ([www.ametsoc.org/PUBSReuseLicenses](http://www.ametsoc.org/PUBSReuseLicenses)).

**Capsule Summary:**

A new field campaign focuses on those atmospheric processes, and their connections to the surface and subsurface, that dominate mountainous hydrology in the Upper Colorado River Basin.

## **Abstract**

The science of mountainous hydrology spans the atmosphere through the bedrock and inherently crosses physical and disciplinary boundaries: land-atmosphere interactions in complex terrain enhance clouds and precipitation, while watersheds retain and release water over a large range of spatial and temporal scales. Limited observations in complex terrain challenge efforts to improve predictive models of the hydrology in the face of rapid changes. The Upper Colorado River exemplifies these challenges, especially with ongoing mismatches between precipitation, snowpack, and discharge. Consequently, the U.S. Department of Energy's (DOE) Atmospheric Radiation Measurement (ARM) user facility has deployed an observatory to the East River Watershed near Crested Butte, Colorado between September 2021 and June 2023 to measure the main atmospheric drivers of water resources, including precipitation, clouds, winds, aerosols, radiation, temperature and humidity. This effort, called the Surface Atmosphere Integrated Field Laboratory (SAIL), is also working in tandem with DOE-sponsored surface and subsurface hydrologists and other federal, state, and local partners. SAIL data can be benchmarks for model development by producing a wide range of observational information on precipitation and its associated processes, including those processes that impact snowpack sublimation and redistribution, aerosol direct radiative effects in the atmosphere and in the snowpack, aerosol impacts on clouds and precipitation, and processes controlling surface fluxes of energy and mass. Preliminary data from SAIL's first year showcase the rich information content in SAIL's many data-streams and support testing hypotheses that will ultimately improve scientific understanding and predictability of Upper Colorado River hydrology in 2023 and beyond.

## **Epigraph**

*“Do not forget that everything in our subject comes from the observations.”*

*-- Carl-Gustaf Rossby advising Victor P. Starr circa 1938 on balancing theory vs. data collection in Newell, Reginald E., et al. 1972: *The General Circulation of the Tropical Atmosphere and Interactions with Extratropical Latitudes, Volume I*. MIT Press, Cambridge, MA.*

## 1. **Introduction:**

High up in the Rocky Mountains, the Colorado River begins its more than 2,300 km journey to the Gulf of California, forming the seventh largest drainage in North America (640,000 km<sup>2</sup>). This river currently provides water resources for numerous ecosystems and 40 million people, creates 15 million jobs, delivers at least 53 gigawatts of hydroelectric capacity, and annually enables \$1.3 trillion of economic activity across the region [[James et al, 2014](#)]. The Colorado River has been the breath of life into the arid Southwestern United States.

However, Colorado River water resources are under extreme pressure. The long-term declines in snowpack in the West [[Mote et al, 2018](#)] has been felt in the 280,000 km<sup>2</sup> of the Colorado River Basin above Lee's Ferry, often referred to as the Upper Colorado River Basin (UCRB) [[McCabe and Wolock, 2009](#)], . The UCRB generates 90% of the Colorado River's total flow [[McCabe and Wolock, 2007](#); [Lukas and Payton, 2020](#)], and so changes in snowpack have been shown to contribute, at least partially, to decreases in stream and river discharge in the Basin [[Milly and Dunne, 2020](#)]. Recently, these trends were punctuated by a drought without precedent in the last 1,200 years [[Williams et al, 2022](#)], which ravaged the Southwest and led to comparisons with even greater droughts in the 2nd Century AD [[Gangopadhyay et al, 2022](#)]. In 2021, the decreases in Colorado River discharge and concomitant drop in reservoir levels were without historical precedent and effectively led to the first ever Level 1 Shortage Condition declaration at Lake Mead [[Santos, 2021](#)]. These events highlighted the urgent need to understand the sensitivities of coupled atmosphere-through-bedrock processes that together determine water resources supply and the possibility of sustainable water governance [[Gerlak et al, 2021](#)].

Both scientific understanding and forecasters' abilities to predict the response of the Colorado to changing hydroclimatic conditions need improvement, especially when this response is sensitive to seasonal hydrometeorology and multi-year effects. For example, forensic analysis of what exactly occurred in 2021 is ongoing, since precipitation and peak snowpack during Water Year 2021 (WY21) were 70% and 50-80% of the 1990-2020

average in the Upper Colorado, respectively, while streamflow and unregulated discharge into Lake Powell were 8 - 57% and 28% of the 1990-2020 average, respectively [[Bailey et al., 2021](#)]. While discrepancies between precipitation and discharge have happened in the past [[Xiao et al., 2018](#)], explanations for such discrepancies in WY21 include (1) lack of April precipitation, (2) snow sublimation, (3) evapotranspiration, (4) dry antecedent soil moisture from drought in previous years, and (5) an overestimation of winter snowpack from sparse observations [[Abatzoglou et al., 2021](#)], with [[Börk et al., 2022](#)] suggesting dry soils as a primary culprit. Regardless, this mystery highlights how a range of processes interact to control the hydrological output of the Upper Colorado River and water availability in the Southwestern United States.

For systems as large and complex as the Colorado River, comprehensive observations from the atmosphere through to the bedrock are limited, so the path forward to improving the forecasting of water resources on weather-to-climate scales is challenged. The scope of this challenge was highlighted recently by [Lundquist et al., \[2019\]](#), who noted that, in complex terrain, it is not straightforward to rely solely on information from a small set of operational observations to understand the spatiotemporal heterogeneities in mountainous hydrologic cycle processes. Rather, joint efforts must focus on observations and modeling in tandem. Data collection and scientific research that cross disciplinary boundaries and integrate atmospheric research are needed. This is especially the case when and where atmospheric science is treating the surface as a boundary condition, and surface/subsurface research is treating the atmosphere as a boundary condition.

Consequently, the scientific community has repeatedly requested simultaneous measurements of energy and water fluxes within complex terrain, due to the need for such data to advance the scientific understanding of the hydrological processes that dominate the uncertainty in the management and prediction of water resources [[Lundquist et al., 2003](#); [Bales et al., 2006](#); [Henn et al., 2016](#); [Lundquist et al., 2015](#); [Henn et al., 2018](#)]. In response to these repeated requests, and also recognizing the programmatic interests in advancing understanding of atmospheric science processes in high-altitude complex

terrain [[U.S. DOE, 2019](#)], the U.S. Department of Energy's Atmospheric Radiation Measurement (ARM) user facility [[Mather and Voyles, 2013](#)] has deployed the Second ARM Mobile Facility (AMF-2) to the Upper Colorado River from September 1, 2021 to June 15, 2023 as part of the Surface Atmosphere Integrated Field Laboratory (SAIL). The AMF-2 includes dozens of instruments (see [Table 1](#)) that broadly measure precipitation, aerosols, clouds, surface fluxes, radiation, atmospheric thermodynamic and kinematic state, and trace gasses. The AMF-2, together with other AMFs, has a rich history of targeted, science-driven deployments to collect detailed, long-term atmospheric observations that target uncertain atmospheric processes that significantly impact Earth System Model projections and address questions that the scientific community is simply unable to address without such a level of detail [[Miller et al., 2016](#)].

The atmospheric processes that fundamentally control water availability in mountain watersheds vary in space and time. Until scientists can understand and produce predictions, with improved skill, of precipitation, aerosols, and surface energy budget fields, the atmosphere will remain a dominant source of uncertainty for surface and subsurface hydrological science. Leveraging the AMF-2's capabilities, SAIL main goal is to advance the predictive understanding of the atmospheric processes driving the mountain hydrology of the UCRB by answering the following science questions (SQ) for the UCRB:

- SQ-1. How do multi-scale dynamical and microphysical processes control the spatial and temporal distribution, phase, amount, and intensity of precipitation in complex terrain that generates local circulations and can modify synoptic weather features?
- SQ-2. How much do aerosols, particularly long-range transported dust and smoke aerosols from wildfires of the Rocky mountains, affect the surface energy and water balance by altering clouds, precipitation, and surface albedo, and how do these impacts vary seasonally?

- SQ-3. At high elevations (>3000 masl) in mid-latitude continental interior mountains, what are the contributions of snow sublimation, radiation, and turbulent fluxes of latent and sensible heat to the water and energy balance of the snowpack?
- SQ-4. How do atmospheric and surface processes set the net radiative absorption that is known to drive the regional flow of water into the continental interior during the summer monsoon?

These questions allow SAIL to focus on science objectives that produce a detailed understanding of water and energy budgets in this region, which are fundamentally the issue for UCRB hydrology research. SQ-1 recognizes that the synoptic and local-scale circulations, and their interactions, all of which are strongly impacted by the terrain, may be central to understanding where and why precipitation varies across the terrain. SQ-2 recognizes that aerosol research is central to UCRB hydrology research and that dust and smoke are the major (but by no means only) sources of aerosols in the region. SQ-3 focuses on a number of surface processes that may impact UCRB hydrology, which may be specific to high-altitude, mid-latitude continental interior mountain ranges because snow conditions, humidity, and radiation are specific to those areas. Finally, SQ-4 focuses on the North American Monsoon as it impacts the UCRB. Following these questions, the collection of data and associated science activities for SAIL are organized around a set of interconnected science objectives (SO):

- SO-1. Characterize the spatial distribution of orographic and convective precipitation processes on diurnal to seasonal time-scales and how those processes interact with large-scale circulation.
- SO-2. Quantify cold-season land-atmosphere interactions that alter snowpack mass balance through wind redistribution and sublimation and the spatial scaling of those processes.
- SO-3. Establish aerosol regimes, the processes controlling the life cycle of aerosols in those regimes, and quantify the impacts of aerosols in those regimes on the atmospheric and surface radiative budget.

- SO-4. Quantify the sensitivity of cloud phase and precipitation to cloud condensation nuclei (CCN) and ice nucleating particle (INP) concentrations.
- SO-5. Quantify the seasonally-varying surface energy balance (SEB), the land-surface and atmospheric factors controlling it, and the spatial variability in those factors.

The rationale behind SAIL's science questions and objectives is that they are designed to seek a deeper understanding of how atmospheric processes impact the seasonal budgets of surface energy and mass because such understanding is central to predicting watershed function [[Lundquist et al., 2003](#); [Bales et al., 2006](#); [Henn et al., 2016](#); [Lundquist et al., 2015](#); [Henn et al., 2018](#)]. It should be noted, though, that both the science questions and objectives of SAIL are not meant to limit scientific inquiry with the SAIL data, but they do guide the campaign's data collection.

While the AMF-2 collects atmospheric state information, SAIL is an interdisciplinary hydrology campaign that spans the atmosphere through the bedrock, crossing the stratosphere, troposphere, canopy, surface, and subsurface. Indeed, the campaign name purposefully highlights its integrated science questions and objectives. Consequently, SAIL works closely with the dozens of surface and subsurface hydrologists whose research is focused on the very same study area as SAIL through the DOE-sponsored Watershed Function Scientific Focus Area (SFA) [[Hubbard et al., 2018](#); [2020](#)]. The combined efforts of SAIL, the Watershed Function SFA, and partners produce atmosphere-through-bedrock observations and modeling to capture the dominant couplings between the atmospheric and hydrologic processes [[Bales et al., 2006](#); [Viviroli et al., 2011](#); [Lundquist et al., 2015](#); [Clark et al., 2015a,b](#)].

This paper first describes the SAIL campaign, revealing connections between SAIL measurements and SAIL science objectives. Second, it touches on key partnerships that augment SAIL's science and leverage its measurements. Third, it presents examples of how SAIL observations are helping achieve its science objectives. Finally, it discusses findings

from the campaign to date and discusses how data collected so far suggest hypotheses that can be tested with end-of-campaign data observations.

## 2. Campaign Description:

The SAIL campaign consists of the deployment of the AMF-2, and, since ARM is a National User Facility, several guest instruments, across the East River Watershed (ERW). The East River is one of the two main tributaries of the Gunnison River, and the Gunnison accounts for just under half of Colorado River discharge at the Colorado-Utah border [Hubbard et al, 2018]. The 300 km<sup>2</sup> ERW area is located near Crested Butte and Gothic, Colorado ([Figure 1](#)), and at its high altitude with high-altitude (2440 – 4350 masl), this watershed is generally snow-dominated, though warm-season convective precipitation associated with the North American Monsoon also contributes. The mean diurnal cycle of temperature ranges from -20 °C to -1 °C in the winter and +3 °C to +23 °C in the summer [[Hubbard et al, 2018](#); [NRCS, 2022](#)]. The ERW, outlined in [Figure 2](#), is marked by large north-south gradients (north is higher) in precipitation, with snowfall ranging from ~500 to ~1000 cm per year, with a coefficient of variation of 19%.

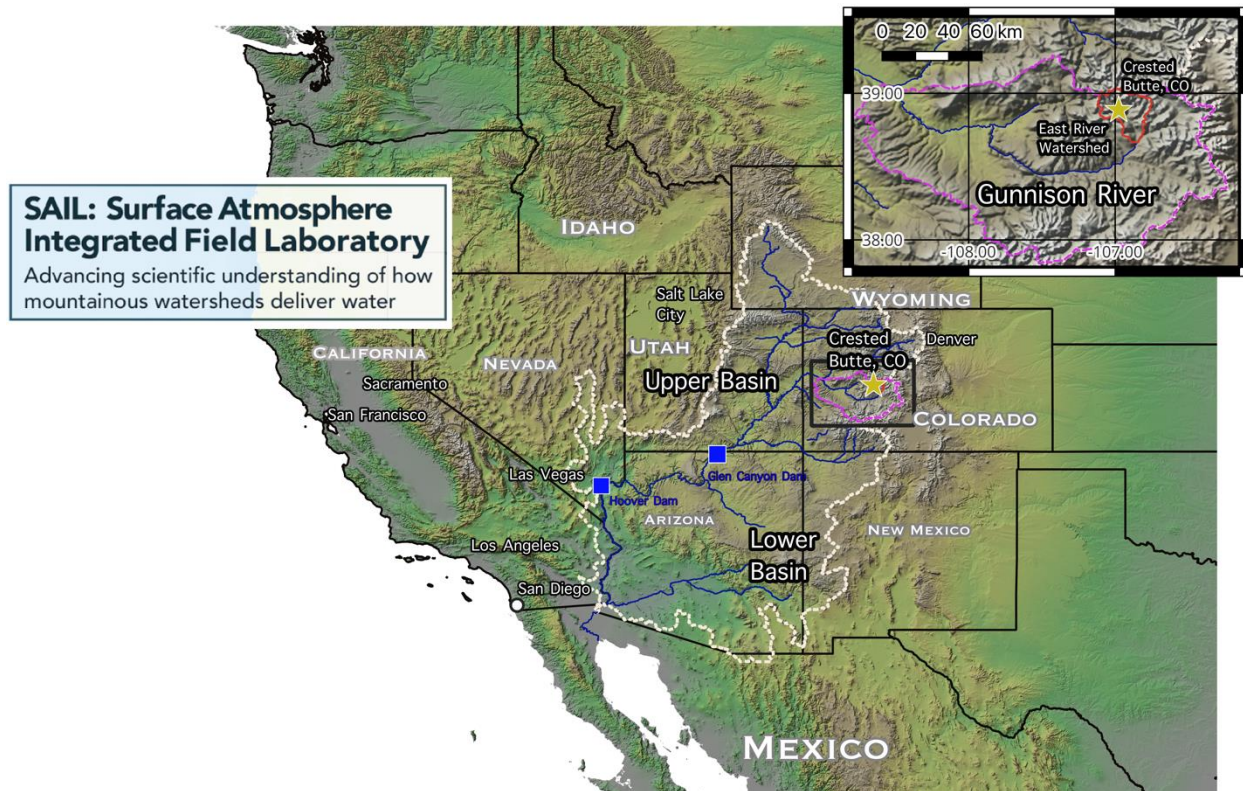


Figure 1: Location of SAIL in the Colorado River Watershed and, in the inset, the Gunnison River Watershed.

SAIL instrument locations ([Figure 2](#)) were selected to enable data collection that supports SAIL science objectives, within logistical limitations. Most SAIL instruments are located at the main site (M1) in the town of Gothic, which is home to the Rocky Mountain Biological Laboratory (RMBL). M1 sits in a valley location immediately adjacent to the East River (38°57'22.35"N, 106°59'16.66"W at 2885 masl). The M1 location provides a detailed set of measurements of a mountain valley and leverages (and helps contextualize) the long-term data records that RMBL has collected, some of which date back to 1928 (see Supplemental Material). A supplemental site (S2) was established beginning October, 2021 at an elevated location (38°53'52.66"N, 106°56'35.21"W at 3137 masl) on the Crested Butte Mountain Resort, where the Aerosol Observing System and a Colorado State University X-band scanning precipitation radar were deployed. It is ~7.5 km south-southeast (SSE) of M1 and was chosen both because its prominence enables broad spatial coverage for the remote sensing observations of precipitation, and because this location enables the sampling of upper-level, regional airflow for aerosol observations. Another supplemental location (S3) has also been established to measure surface fluxes of sensible and latent heat at 3m AGL over an area covered in short grass and is located 2 km SSE of that site at Kettle Ponds (38°56'29.55"N, 106°58'23.34"W). The S3 location was chosen because of the need to look at heterogeneity in those surface fluxes and the lack of homogenous/unobstructed fetch at M1. Finally, the SAIL campaign has also deployed the Tethered Balloon System (TBS) [[Dexheimer et al, 2019](#)] to augment measurements at the 3 SAIL sites with in situ vertical profile sampling of the lowest 1000-m of the atmosphere, and also visible/thermal imaging (see Table 2 for details). The TBS has been deployed within 200 m of M1 in September 2021, May 2022, and July 2022 and has plans for three two-week deployments in January, March and May, 2023 at the banks of the East River 3.0 km SSE of S3 at the Pumphouse (PH) site (38°55'19.98"N, 106°57'3.95"W at 2765 masl).

Table 1: SAIL AMF-2 Instruments, with more instrument details in Supplemental Material and [Mather and Voyles, 2013].

Instrument	What it Measures	Dimensions of Observation (X= east-west, Y= north-south, Z= vertical	Spatial Resolution	Max Range / Footprint	Temporal Resolution	Location	Science Objective
Aerosol Chemical Speciation Monitor ( <a href="#">ACSM</a> )	Mass concentrations of organics, sulfate, nitrate, ammonium, and chloride in surface-deposited aerosols.	Point observation	N/A	N/A	10 min	S2	<a href="#">3</a>
Aerosol Observing System Meteorology Station ( <a href="#">AOSMET</a> )	Humidity, temperature and winds to aid analysis of aerosol observations.	Point observation	N/A	N/A	1 sec	S2	<a href="#">3</a> , <a href="#">4</a> , <a href="#">5</a>
Atmospheric Emitted Radiance Interferometer ( <a href="#">AERI</a> )	Derived vertical profiles of atmospheric temperature and humidity from scans in the X-Z plane.	Z, X	100 m	10 km	30 sec	M1	<a href="#">2</a> , <a href="#">5</a>
Carbon Monoxide Monitoring System ( <a href="#">CO</a> )	Carbon monoxide mixing ratio at the surface.	Point observation	N/A	N/A	1 min	S2	<a href="#">3</a>
Ceilometer ( <a href="#">CEIL</a> )	Planetary boundary layer height, cloud base height, vertical visibility, atmospheric backscatter.	Z	10 m	7.5 km	16 sec	M1	<a href="#">2</a> , <a href="#">5</a>
Cloud Condensation Nuclei Counter ( <a href="#">CCN</a> )	Cloud condensation nuclei number concentration at the	Point observation	N/A	N/A	1 sec	S2	<a href="#">3</a> , <a href="#">4</a>

	surface at super-saturations from 0.0 to 0.8.											
Cimel Sunphotometer ( <a href="#">CSPHOT</a> )	Direct solar irradiance and sky radiance at the Earth's surface.	Point observation	N/A	N/A	1 min	M1						<a href="#">5</a>
Condensation Particle Counter ( <a href="#">CPC</a> )	Sub-micron aerosol particle number concentration.	Point observation	N/A	N/A	1 sec	S2						<a href="#">3</a>
Disdrometer (LDIS)	Surface precipitating hydrometeor particle size distribution and fall speed.	Point observation	N/A	N/A	1 min	M1, S2						<a href="#">1</a>
Doppler Lidar ( <a href="#">DL</a> )	Horizon-to-horizon 3-D radial wind velocities at 1-degree zenith/azimuth angle resolution	X, Y, Z	30 m	10 km	30 sec	M1						<a href="#">2</a>
Eddy Correlation Flux Measurement System ( <a href="#">ECOR</a> )	Turbulent fluxes of momentum, latent and sensible heat.	Point observation	N/A	< 1 km	30 min	M1, S3						<a href="#">2</a> , <a href="#">5</a>
Filters for collecting Ice Nucleating Particle Spectra ( <a href="#">INS</a> )	Immersion freezing temperature spectra of ice-nucleating particles.	Point observation	N/A	N/A	2x weekly	S2						<a href="#">4</a>
Ground Radiometers on Stand for Upwelling Radiation ( <a href="#">GNDRAD</a> )	Surface upwelling shortwave and longwave broadband radiative fluxes.	Point observation	N/A	N/A	1 min	M1						<a href="#">2</a> , <a href="#">3</a> , <a href="#">5</a>

High Spectral Resolution Lidar ( <a href="#">HSRL</a> )	Vertical profiles of optical depth, backscatter cross-section, depolarization, and backscatter phase function.	Z	7.5 m	30 km	5 sec	M1	<a href="#">2</a> , <a href="#">3</a>
Humidified Tandem Differential Mobility Analyzer ( <a href="#">HTDMA</a> )	Aerosol particle hygroscopicity.	Point observation	N/A	N/A	10 min	S2	<a href="#">3</a>
Infrared Thermometer ( <a href="#">IRT</a> )	Surface skin temperature.	Point observation	N/A	N/A	1 min	M1	<a href="#">2</a> , <a href="#">5</a>
Ka Band Zenith Radar ( <a href="#">KAZR</a> )	Vertically-resolved cloud particle profiles, their Doppler velocity, reflectivity, and spectral width at Ka band frequencies.	Z	30 m	20 km	2 sec	M1	<a href="#">1</a>
Micropulse Lidar ( <a href="#">MPL</a> )	Aerosol and cloud location and scattering property profiles, hydrometeor phase.	Z	15 m	18 km	10 sec	M1	<a href="#">2</a> , <a href="#">3</a> , <a href="#">5</a>
Microwave Radiometer ( <a href="#">MWR</a> , <a href="#">MWR3C</a> )	Total column liquid water in clouds and total column gaseous water vapor.	Point observation	N/A	N/A	1 sec	M1	<a href="#">5</a>

Multi-Filter Rotating Shadowband Radiometer ( <a href="#">MFRSR</a> )	Aerosol optical depth, diffuse and direct radiation, total water vapor.	Point observation	N/A	N/A	1 min	M1	<a href="#">3</a> , <a href="#">5</a>
Nephelometer ( <a href="#">NEPH</a> )	Scattering and hemispheric backscatter of aerosols.	Point observation	N/A	N/A	5 sec	S2	<a href="#">3</a>
Ozone Monitor ( <a href="#">O3</a> )	Surface atmospheric ozone concentration.	Point observation	N/A	N/A	5 sec	S2	<a href="#">3</a>
Particle Soot Absorption Photometer ( <a href="#">PSAP</a> )	Bulk absorption of surface atmospheric aerosols.	Point observation	N/A	N/A	1 sec	S2	<a href="#">3</a>
Radar Wind Profiler ( <a href="#">RWP</a> )	Wind speed and direction profiles from 5 profiles around zenith.	Z (+/-)	10 m	10 km	1 hour	M1	<a href="#">2</a>
Radiosonde ( <a href="#">SONDE</a> )	Profiles of temperature, water vapor, and wind speed and direction.	Z	0.1 m	20 km	12 hours	M1	<a href="#">2</a> , <a href="#">3</a>
Sky Radiometers on Stand for Downwelling Radiation ( <a href="#">SKYRAD</a> )	Surface downwelling shortwave and longwave broadband radiative fluxes.	Point observation	N/A	N/A	1 min	M1	<a href="#">2</a> , <a href="#">3</a> , <a href="#">5</a>
Single Particle Soot Photometer ( <a href="#">SP2</a> )	Surface atmospheric soot mass.	Point observation	N/A	N/A	60 sec	S2	<a href="#">3</a>
Surface Energy Balance System ( <a href="#">SEBS</a> )	Surface upwelling and downwelling solar and infrared	Point observation	N/A	N/A	30 min	M1, S3	<a href="#">2</a> , <a href="#">3</a> , <a href="#">5</a>

	broadband radiation, net radiometer, soil temperature, soil moisture and soil heat flux.								
Surface Meteorology (MET)	Surface air temperature, relative humidity, and wind speed and direction.	Point observation	N/A	N/A	1 min	M1		<a href="#">2</a> , <a href="#">4</a> , <a href="#">5</a>	
Total Sky Imager (TSI)	Horizontal distribution of cloud sky fraction.	X, Y	<45 m	6 km	30 sec	M1		<a href="#">2</a> , <a href="#">5</a>	
Ultra-High Sensitivity Aerosol Spectrometer (UHSAS)	Optical scattering of aerosols to determine their size distribution at the surface.	Point observation	N/A	N/A	10 sec	S2		<a href="#">3</a>	
Weighing Bucket Rain Gauge (WBPLUV)	Surface precipitation.	Point observation	N/A	N/A	1 min	M1		<a href="#">1</a>	
X-Band Polarimetric Weather Radar (XPRECIPRADAR)	Precipitation amount and type, and hydrometeor radial velocities.	X, Y, Z	100 m	50 km	15 min	S2		<a href="#">1</a>	

There are additional intensive sites throughout the ERW, a few of which are shown in [Figure 2](#), including Snodgrass Mountain (38°55'40.63"N, 106° 58'47.07"W at 3169 masl). This site can be accessed year-round, has two weather stations at mid-mountain and the summit, has direct line-of-sight to the Colorado State University (CSU) X-band radar at S2 (see Section 3 and [[McLaughlin et al, 2009](#)] for details), and is the site of intensive vegetation and subsurface observations collected by the Watershed Function SFA, and thus is a location to explore the interactions between precipitation, vegetation, snow, soil, and groundwater conditions, thereby enabling atmosphere-through-bedrock science. Additionally, the National Oceanic and Atmospheric Administration (NOAA) led Study of Precipitation, the Lower Atmosphere and Surface for Hydrometeorology (SPLASH) campaign manages additional intensive sites [[de Boer et al., 2023](#)]. These include the Avery Picnic site, located approximately 2 km north of Gothic; the Kettle Ponds site co-located with S3; and the Brush Creek site, located 5 km SSE of S2. Kettle Ponds is also the location of an upcoming field campaign called Sublimation of Snow (SOS), which is supported by the National Science Foundation and the Earth Observing Laboratory at the National Center for Atmospheric Research. Section 8 covers details of these partnerships.

*Table 2: Instruments Deployed on the Tethered Balloon System (TBS) Platform at SAIL*

Instrument	What it Measures
Vis/Thermal Imager	Spatially-resolved visible and thermal radiance.
Condensation Particle Counter (CPC)	Total aerosol concentration from 0.01 $\mu\text{m}$ to 1 $\mu\text{m}$ .
Met package	Pressure, temperature, relative humidity, wind speed and wind direction.
Portable Optical Particle Spectrometer (POPS)	Aerosol size distribution from 0.14 $\mu\text{m}$ to 3 $\mu\text{m}$ .
Size and Time Aerosol Composition (STAC)	Size and time-resolved chemical composition at four cut-off sizes (0.1-0.5 $\mu\text{m}$ ; 0.5-1.0 $\mu\text{m}$ ; 1-2.5 $\mu\text{m}$ ; and 2.5-5.0 $\mu\text{m}$ ).
IcePuck	Filters for collecting Ice Nucleating Particles (INP).

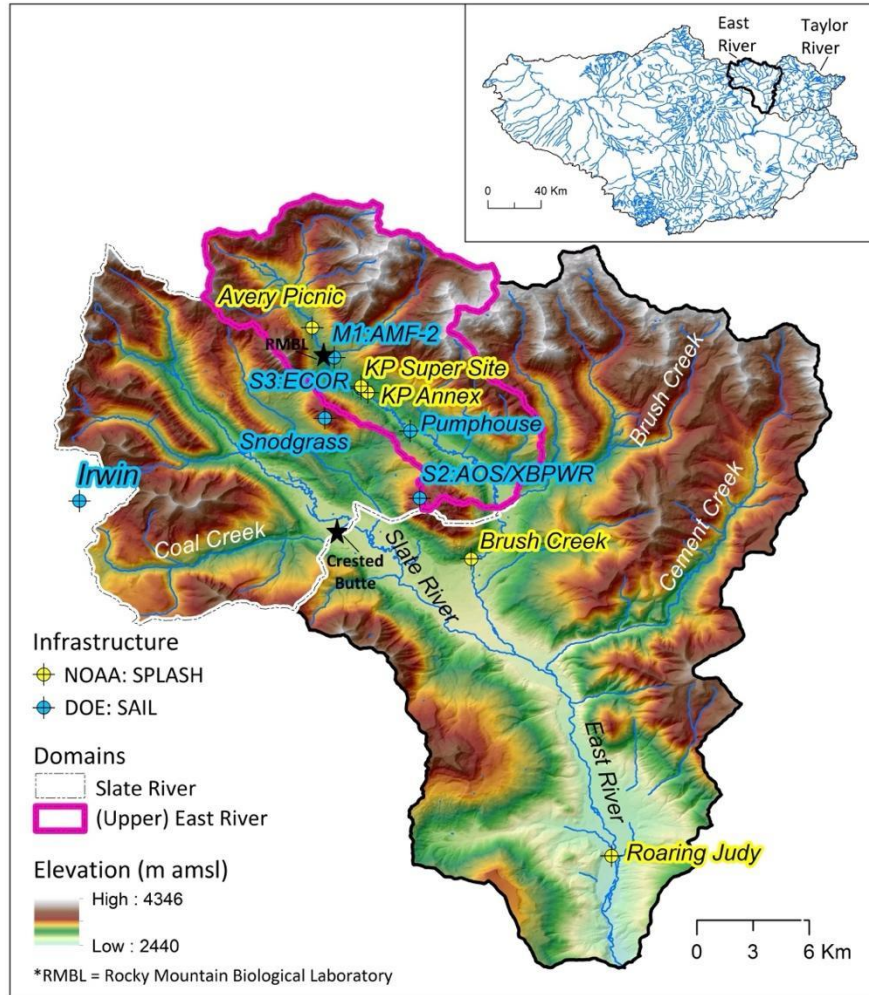


Figure 2: (Upper plot) ERW outline (red) and East River, Slate River, Coal Creek, and Washington Gulch watersheds outline (yellow). Green locations show SAIL M1, S2, and S3 sites and Watershed Function SFA intensive sites at Snodgrass Mountain and the Pumphouse. Yellow icons denotes SPLASH intensive sites. Inset shows ERW within the Gunnison River

Watershed. (Lower left) aerial photograph of M1 in September, 2021. (Lower right) photograph of S2 in November, 2021.

Collocating measurements at a single location enables the exploration of multiple, simultaneous observations of the atmospheric processes and land-atmosphere interactions that are occurring in the ERW. [Figure 3](#) shows how dense, comprehensive observations reveal details about atmospheric and surface processes in high-altitude complex terrain.

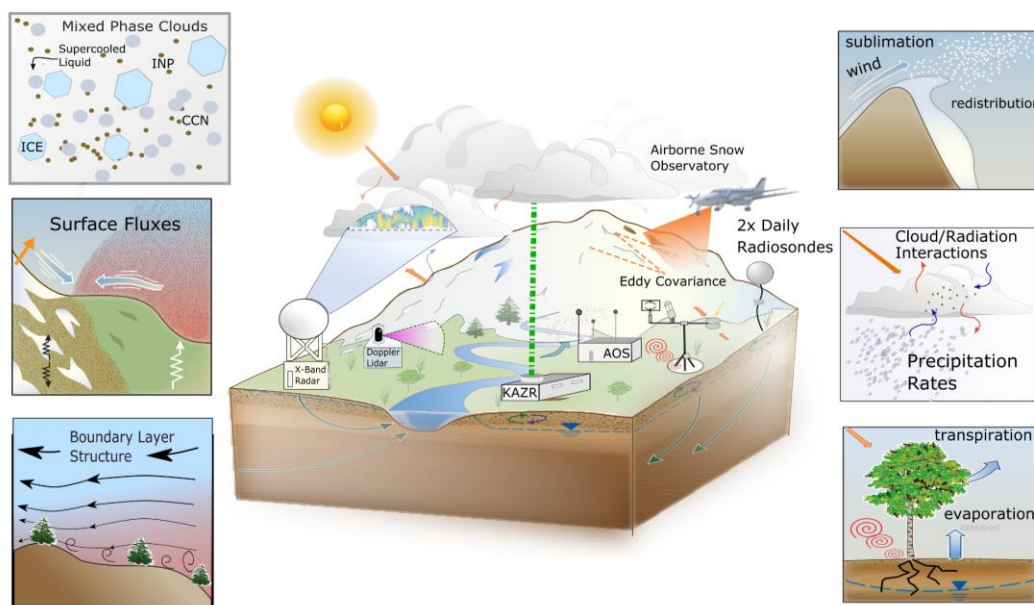


Figure 3: Depiction of multiple observations from SAIL and partners to collect observations of major hydrological processes (called out on left and right) of the ERW.

The connections between each of SAIL’s five science objectives and its datastreams are described in detail, along with examples, below. Each of the SAIL datastreams is free, accessible and interoperable, and comes with a large number of tools to ensure reusability. Since SAIL is supported by ARM, the campaign uses the highly-mature data solutions that the ARM program has developed including a strong chain-of-custody [[McCord and Voyles, 2016](#)], data quality assurance [[Peppler et al, 2016](#)], and a well-maintained interface to freely access data through the ARM Data Discovery [[Guntupally et al, 2021](#)]. The latency with which data becomes available depends on the dataset and current network conditions,

but the fundamental measurements collected from SAIL are generally available for download within a few hours of their collection.

### **3. Precipitation Processes and Quantitative Estimates:**

The surface water balance in mountainous terrain is strongly driven by the amount and phase of precipitation (e.g., [Hamlet et al. \[2007\]](#), [Berghuijs et al. \[2014\]](#), [Li et al. \[2017\]](#), [Musselman et al. \[2017; 2018\]](#)). However, the spatial and temporal details of observed precipitation amount and phase in mountain environments is poor in comparison to less topographically-complex locations [[Henn et al., 2018](#)]. Operational weather radar coverage in the mountain regions of the continental United States suffers from radar beam blockage [[Maddox et al, 2002](#); [National Research Council, 2002](#)], often resulting in no data in the lowest several kilometers of the atmosphere where precipitation can grow or evaporate. Further, orographic circulations significantly modify precipitation where these data gaps exist. The precipitation amount and phase across much of the Rocky Mountains is currently estimated from a combination of operational network point observations, Integrated Multi-satellitE Retrievals for Global Precipitation Measurement (IMERG) satellite retrievals that use snapshots from spaceborne radar and microwave radiometers, in combination with statistical and physics-based modeling that assimilates some of those data. Unfortunately, there is a strong potential for biases from point observations, since steep slopes, high elevations, and forested sites are underrepresented in the measurement network (e.g., [Sevruk, \[1997\]](#); [Frei and Schär, \[1998\]](#); [Henn et al., \[2018\]](#)), and gauge undercatch of precipitation is ubiquitous, particularly for snowfall (e.g., [Pan et al. \[2003\]](#); [Rasmussen et al., 2012](#)). Interpolating between point observations has been found to depend strongly on the number, type, and spatial/elevational distribution of observations [[Zhang et al., 2017](#)] and to be the most important source of rainfall/runoff model errors [[Moulin et al., 2009](#); [Lundquist et al., 2019](#)]. Meanwhile, satellite precipitation estimates in complex terrain also often have significant biases due to an inability to retrieve data at and below the altitudes of mountain peaks [[Barros and Arulraj, 2020](#)].

SAIL's Science Question 1 ([SQ-1](#)) and Science Objective 1 ([SO-1](#)) focus on understanding how and why precipitation varies at the scales of watersheds like the East River with the goal of understanding how and why precipitation varies over the entire UCRB.

In the UCRB, there are highly variable, multiscale dynamical, thermodynamical, and microphysical factors that interact to control orographic precipitation. Orographic circulations create clouds by inducing ascent through a variety of mechanisms depending on combinations of the air flow speed and direction impinging on the barrier, atmospheric thermodynamic stability, surface fluxes, and the barrier shape [[Houze, 2012](#); [Stoelinga et al., 2013](#)]. Once clouds form, an array of microphysical processes respond to and interact with atmospheric circulations, turbulence, and aerosols to control the phase, growth, evaporation, and fallout of hydrometeors that dictate precipitation location, phase, and intensity at the surface. And yet, despite this complexity, repeating patterns emerge: the ERW likely experiences large precipitation gradients as evidenced by persistently large snowpack gradients observed in airborne snow surveys [[Painter et al., 2016](#)] and SNOTEL station data [[Serreze et al., 1999](#)], with twice as much snow at its northern edge as compared to the southern edge at the same elevation.

SAIL observations enable detailed explorations of that emergent phenomenon by looking at the underlying atmospheric conditions and precipitation types that produce this sharp gradient. The CSU radar at the S2 site is a scanning dual-polarization Doppler X-band (9.4-GHz) radar that collects observations with a 1.25° beam width and 100-m gate spacing to a range of 50 km where beams are not blocked. The radar's 10-minute scan sequence includes a volume derived from Plan Position Indicator (PPI) scans at 8 elevation angles to map precipitation across the study domain, and 7 Range-Height Indicator (RHI) scans within 3° of the azimuthal direction of M1. The RHI scans provide detailed context to the multitude of point and profile measurements at M1. Dual-doppler retrievals are also achieved with an identical radar deployed as part of SPLASH at the Roaring Judy Fish Hatchery (38°43'0.78"N, 106°51'10.98"W), which is 21.6 km SSE of S2.

[Figure 4](#) provides an example of precipitation process insights provided by the multivariate observations collected as part of SAIL for a single storm on 12 April 2022. The precipitation began with virga that evaporatively cools low-level temperatures over time. Cooling and moistening was most apparent between 8 and 10Z when the precipitation rate was most intense ([Figure 4a](#)) and cloud base lowers (along with a cooling of 2-m air temperatures) ([Figure 4b](#)). This, along with deepening and intensifying convective graupel precipitation indicated by sharp reflectivity gradients ([Figure 4a](#)), significant supercooled liquid water path, and substantial downward velocities ([Figure 4b](#)) allows precipitation to reach the surface and accumulate. The X-band radar shows that these showers advected in from the west ([Figure 4f](#)) and the operational NEXRAD radar to the west confirms these showers were initiating as westerly flow rises over the high ridgeline to the west of Crested Butte. Southwesterly winds above the ridgeline were strong ahead of the front, reaching 30-35 m s<sup>-1</sup> just above Gothic Mountain, though notably less in the valley with strong turbulence indicated by high spectral width ([Figure 4c](#)) and southeasterly winds at low levels ([Figure 4d](#)), likely due to the storm system flowing up the valley.

Cold frontal precipitation began just after 12Z and occurred for several hours until the upper levels stabilize, as evidenced by the widening height gap between -20 and -40°C ([Figure 4a](#)). When the frontal precipitation started at 12Z and winds shifted to north-northwest ([Figure 4d](#)), the cloud base quickly lowered to just above the surface ([Figure 4b](#)). The precipitation rate was most intense during this period through about 1430Z ([Figure 4a](#)). The lesser downward velocities ([Figure 4c](#)) and spectral widths ([Figure 4d](#)) with more horizontally uniform reflectivity and sharp reflectivity gradient in the -10 to -20 °C region ([Figure 4a](#)) indicate that this was heavy snow driven by dendritic growth, likely supporting heavier snow in the valley than at higher elevations during this time period given the low cloud base. There were also more steady updrafts during this period in the upper portions of clouds reaching nearly 9 km asl ([Figure 4b](#)), though there were still embedded convective circulations affecting precipitation variability. Precipitation after 14Z shifted to broken convective showers with much lesser precipitation rates ([Figure 4a](#)). Supercooled liquid also was not detectable. This was associated with upper-level

stabilization and drying ([Figure 4b](#)), though low-level lapse rates remained steep, with cold air supporting light convective showers with little surface accumulation ([Figure 4a](#)). Turbulence remained strong at the ridgeline during this period ([Figure 4b](#)), probably associated with the background wind interaction with the mountains. The X-band radar showed these showers were generated over the high ridgelines ([Figure 4](#), bottom panel).

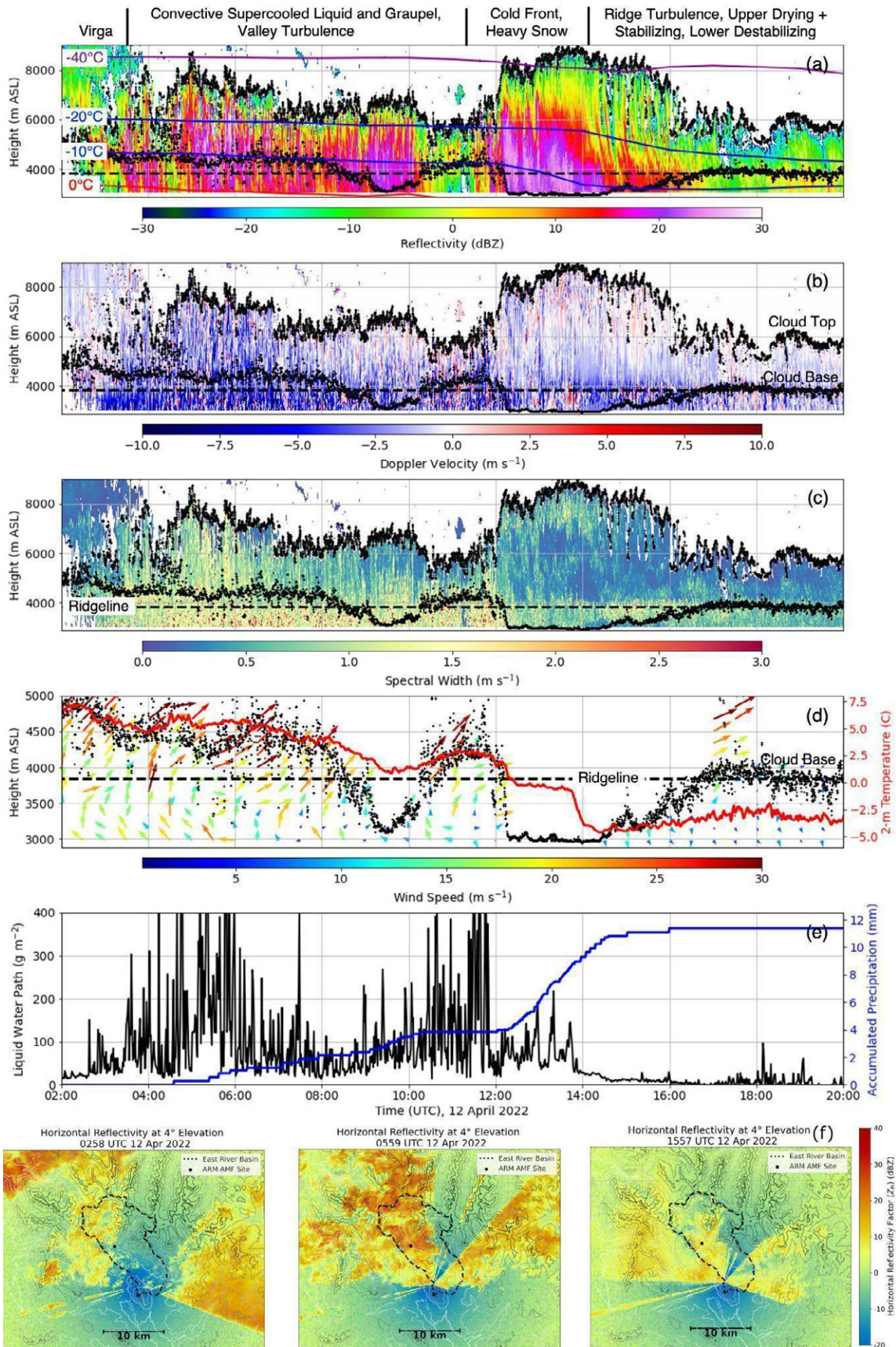


*Figure 4: Time-heights of (a) reflectivity, (b) Doppler velocity, and (c) Doppler spectral width measured by KAZR for April 12, 2022 cloud bases and tops (black +’s) and the height of Gothic Mountain (dashed black). Isotherms from ERA5 overlain in (a). (d) Time-height of Doppler lidar derived horizontal winds. (e) MWR retrieved liquid water path and 24-hour accumulated liquid equivalent precipitation. (f) CSU X-band PPI snapshots of the virga, convective graupel and ridge enhanced precipitation regimes noted at the top of the figure.*

Radar precipitation retrievals are also critical to advancing the scientific understanding of ERW hydrometeorology. While such retrievals are an area of active research, the Corrected Moments in Antenna Coordinates 2.0 product (CMAC2.0) [Collis et al, 2018] is used to estimate snowfall rates through various radar Z-S relationships defined within existing literature [Wolfe and Snider, 2012]. That Z-S relationship agrees favorably with one tuned to a Parsivel disdrometer. Figure 5 shows a time-height cross-section of the X-band radar reflectivity (top panel) over M1 while the disdrometer shows the evolution of the disdrometer-retrieved particle size distribution. This example highlights the rapid temporal variability in snowfall rates (e.g., near 0300Z shown with the vertical dotted line), along with significant variability in different Z-S estimates with one of the Z-S relationships agreeing well with in situ measurements.

SAIL datasets enable investigation into the relative contributions of different precipitation phases to annual snow and water budgets, including controls of temperature, relative humidity, orographic flows, and turbulence on precipitation phase and evaporation. They also allow investigations of how different precipitation regimes (e.g., snowfall, warm rain) vary as a function of mesoscale and synoptic circulations. Detailed observations of these precipitation processes over many events with variable meteorological conditions will support evaluation of model parameterizations of varying scales and complexities, facilitating the improved prediction of precipitation across the Upper Colorado River Basin and other mountain regions. These datasets can also serve as benchmarks to set research and development priorities for Earth System Modeling development, such as robust sub-

grid parameterizations of clouds and precipitation in complex terrain that reflect the underlying processes that are occurring in those systems.

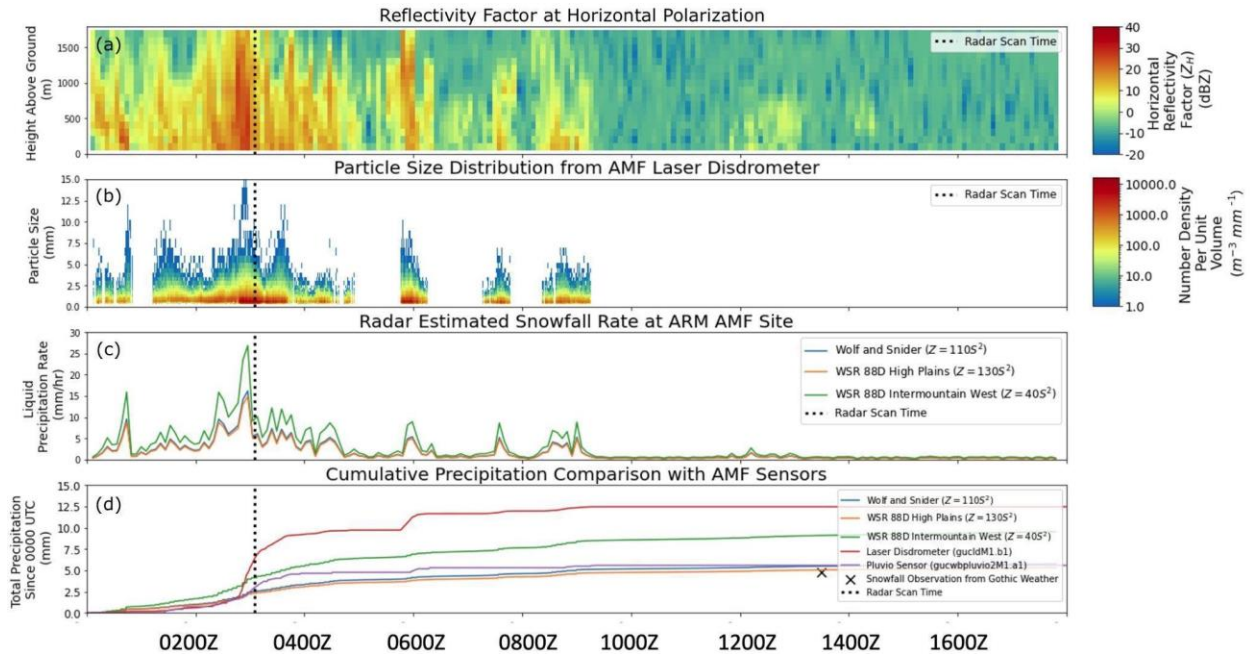


Figure 5: (a)  $Z_H$  column from the CSU X-band radar 14 March 2022 over M1. (b) Parsivel hydrometeor size distribution time-series at M1 with unreliable high wind speed times removed. (c) Three snowfall liquid water equivalent retrievals from the CSU X-band radar. (d) Daily accumulation of retrievals shown in (c), a Pluvio-2 weighing bucket gauge, and a daily snow stake measurement at Gothic (marked as ‘X’).

#### 4. **Snow Sublimation and Wind Redistribution:**

SAIL’s Third Science Question ([SQ-3](#)) and Second Science Objective ([SO-2](#)) focus on sublimation of snow and its redistribution by winds, as these processes substantially impact mountainous hydrology [[Hood et al, 1999](#); [Sextstone et al, 2016](#); [Mott et al., 2018](#)]. Unfortunately, observational estimates of snow sublimation disagree with each other wildly [[Mott et al., 2018](#); [Liston and Sturm, 2002](#); [Groot Zwaaftink et al, 2013](#)], ranging from seasonal sublimation losses of 0.1% of snowpack to 25% of the snowpack. The range of loss estimates remains large enough to hinder water resource predictability in the UCRB [[Bruce](#)

*et al, 2012; Sextstone et al, 2016*], but daily snowpack sublimation rates in the Rockies have been estimated to be as high as 5 cm per day [*Fassnacht et al, 2021*].

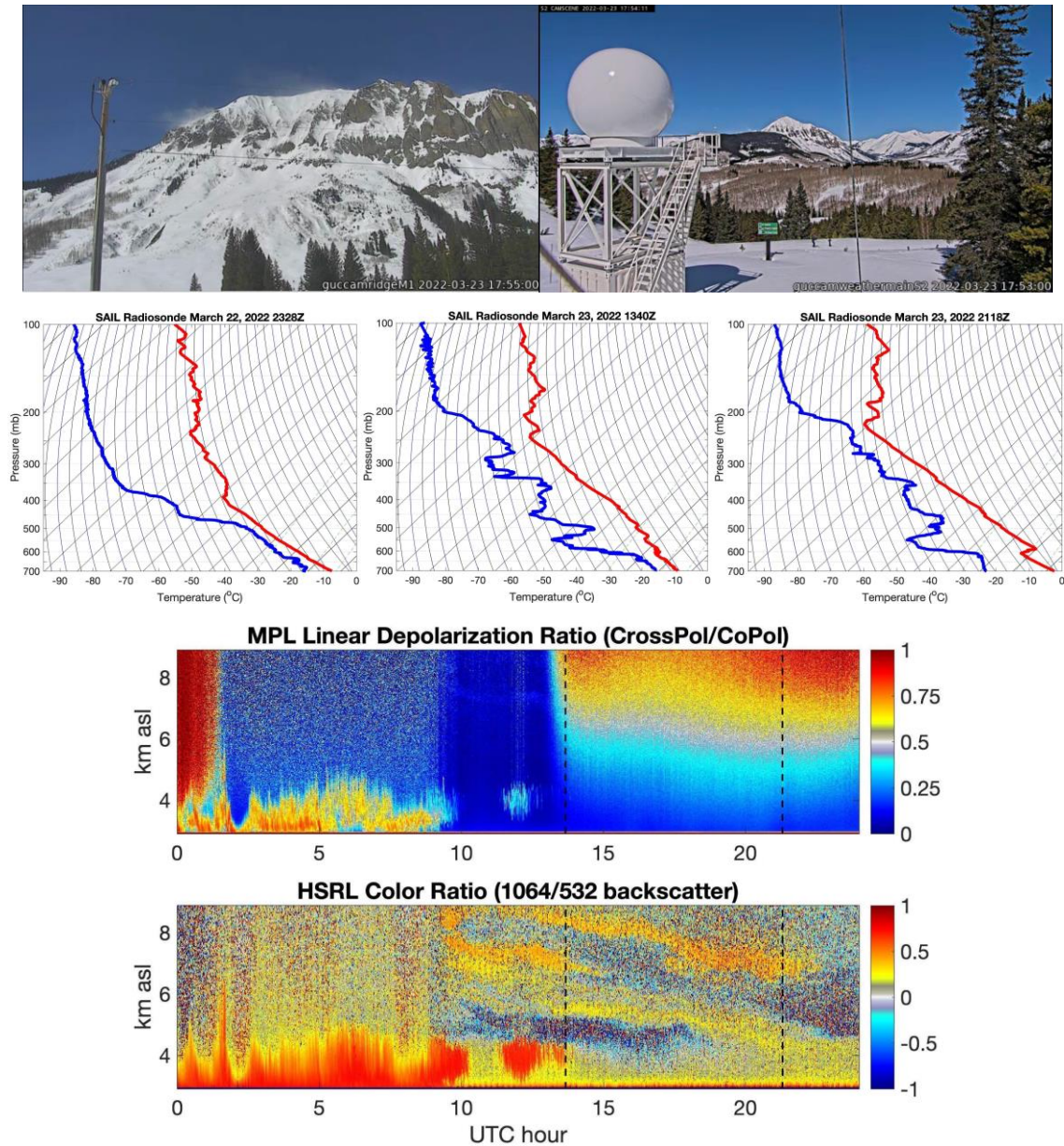


Figure 6: (Top row) Image from camera at S2 on SAIL AOS container of blowing snow (left) directly off of Gothic Mountain and (right) viewing Gothic Mountain from Crested Butte Mountain with the XPRECIPRADAR on the left on March 23, 2022. (Middle row) Three radiosonde skew-T log-P diagrams of temperature (red) and dew-point temperature (blue). (Bottom two rows) The time-series of HSRL linear depolarization ratio (MPL) back-scatter color ratio.

Models ultimately are required to estimate snow sublimation mass losses to the atmosphere, but the thermodynamic feedback on blowing snow sublimation, especially if it can lead to saturation where sublimation is occurring, can limit these losses and is poorly constrained [[Mott et al., 2018](#)].

SAIL is developing observational datasets of some of the fundamental controls on snow sublimation and redistribution in the UCRB. SAIL is collecting data on (1) the three-dimensional atmospheric wind-field across the ERW, (2) surface point measurements and profiles of atmospheric temperature and humidity for sublimation tendencies, and (3) radar measurements to capture snow entrainment and accumulation. The observational information that SAIL's datastreams produce include blowing-snow occurrence, thermodynamics, and radiation and how they co-evolve in space and time (see [Table 2](#) for details), in order to understand better the processes governing snow sublimation (see [[Svoma, 2016](#)] for details).

For example, AMF datastreams provide multiple observational datasets on blowing snow and thermodynamic conditions. [Figure 6](#) shows that blowing snow can be detected on clear-sky days from camera imagery taken from different angles (that indicates that plumes of condensates are entrained snow and not clouds) and also shows the temporal evolution of blowing snow layers (especially from 1000-1400 UTC as shown in [Loeb and Kennedy \[2021\]](#)). This shows how SAIL data enables the ability to understand the thermodynamic environment into which snow is blowing. [Figure 6](#) shows that blowing snow can be detected unambiguously, and may be warming and humidifying the atmosphere below 600 mb, as shown in the 2118Z sonde. Again, multiple datastreams can be used here to estimate sublimation rates.

Another central aspect to snow science at SAIL is the wide variety of collaborative resources described in Section 8. Especially with snow process science, remote sensing

surveys and *in situ* data inform estimates of sublimation losses and associated sensitivities, as described in Section 8.

## 5. **Aerosol Regimes and Their Impacts on Radiation:**

Radiation-absorbing particles such as dust, and black carbon (BC) and brown carbon (BrC) from biomass burning, enhance snowmelt rates by lowering snow surface albedo directly in the visible wavelengths and indirectly in the near-infrared wavelengths by enhancing snow grain growth [[Painter et al., 2007](#)]. Although this has been studied previously, a more holistic view of atmospheric particles that includes radiative impacts of absorbing and scattering aerosol in the air and particles deposited on snow is required to fully understand their roles in mountain water and energy budgets. For example, as the primary absorber of visible light in the atmosphere, atmospheric BC, a product of incomplete combustion, can both reduce the amount of incident irradiance at the snow surface (when present in the atmosphere) and increase the amount of absorbed solar radiation (when present at the snow surface). Snow-deposited absorbing particles tend to decrease atmospheric stability and increase turbulent fluxes, while absorbing aerosols in the air will tend to produce the opposite effect [[Flanner et al., 2009](#); [Hansen and Nazarenko, 2004](#); [Kaspari et al., 2011](#); [Ramanathan and Carmichael, 2008](#)]. BrC aerosols have been implicated as major drivers for cryospheric melt in high-altitude terrain, but are severely understudied [[Laskin et al., 2015](#); [Wu et al., 2016](#)]. Despite the radiative importance of atmospheric aerosol, both suspended in air and deposited on snow surfaces, their energetic impacts are poorly constrained by observations and to date have been primarily informed by models, (e.g., [Bond et al., \[2013\]](#)).

SAIL is developing highly-detailed observations on processes that impact the aerosol regimes and radiation in the ERW as summarized in Science Objective 3 (SO-3) first and foremost with the Aerosol Observing System (AOS) [[Uin et al., 2019](#)]. The AOS, located at S2, is collecting time-resolved data on the aerosol size distribution, hygroscopicity,

composition, aerosol optical properties, and carbon monoxide and ozone trace gasses, along with filter collections to measure INPs. These data, as shown in Figure 7, characterize the state and sources of aerosols in the ERW during a three week period in the spring of 2022 that contains numerous aerosol deposition events. Additionally, remote sensing datastreams are sensitive to the vertical distribution of aerosols and provide information on the relationships between surface observations and aerosol loading in the boundary layer and free troposphere aerosol amounts.

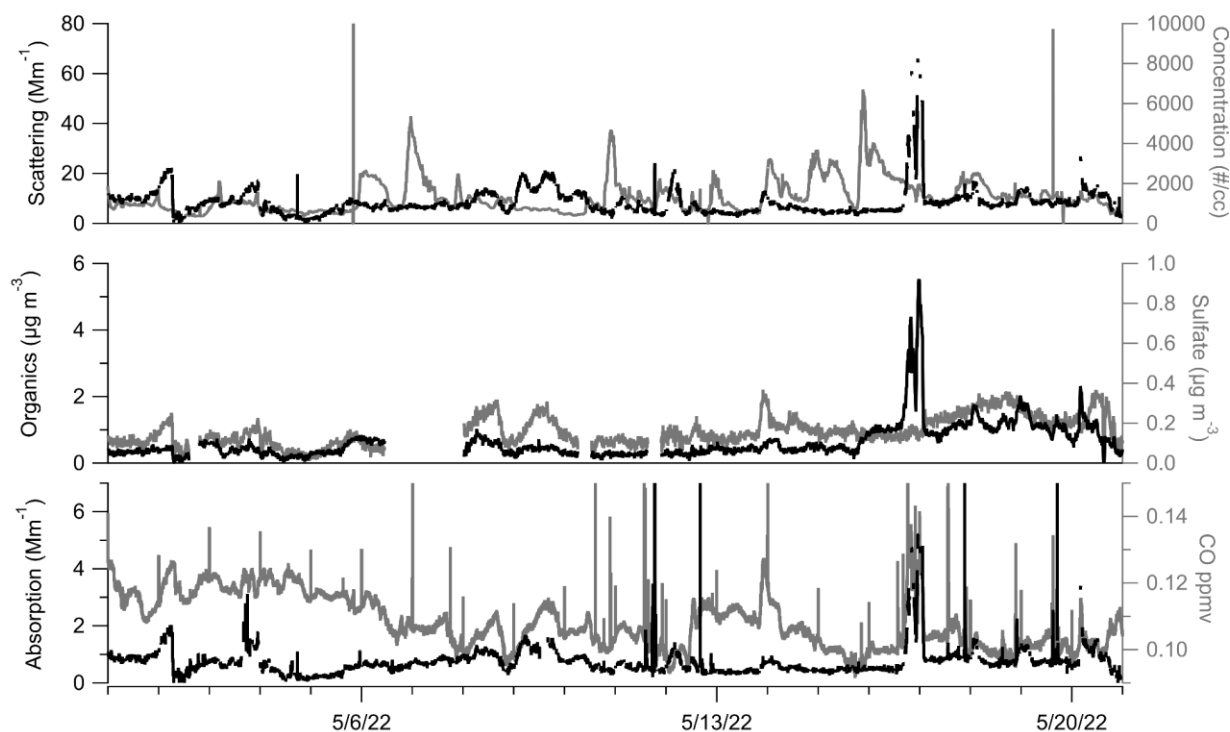


*Figure 7. Submicron aerosol physical, optical and chemical properties as measured by the AOS. (a) Light scattering is shown at 450 nm measured by the nephelometer and number concentrations as measured by the Scanning Mobility Particle Sizer. (b) Organic and Sulfate concentrations as measured by the Aerosol Chemical Speciation Monitor. (c) Light absorption at 470 nm measured by the Particle Soot Absorption Photometer and CO(g).*

To augment and contextualize the time-series of observations at the SAIL AOS, Handix Scientific, Inc. of Fort Collins, Colorado, supported by a U.S. DOE Atmospheric System

Research grant, deployed SAIL-NET, which added six additional aerosol measurement sites to the SAIL domain ([Figure 8](#)). SAIL-NET is designed to test the value of a network of high-quality aerosol measurements and its scientists will work with SAIL scientists and external partners to determine design and measurement successes and areas for improvement.

SAIL-NET provides further insights on aerosol vertical, horizontal, and temporal variability and aerosol-cloud interactions in mountainous terrain in support of SQ-2/SO-4. This partner project takes advantage of the availability of lightweight but still research-grade instruments that can be easily deployed across challenging environments, including off-the-grid remote sites and on the TBS. Each Handix SAIL-NET site consists of an aerosol microphysics package that collects real-time particle size distributions (PSDs) using a Portable Optical Particle Spectrometer (POPS), real-time CCN concentrations from a CloudPuck, and 24 to 48 hour filter samples using an IcePuck for offline INP analysis. SAIL-NET measurement collection is scheduled to run between October 2021-June 2023.

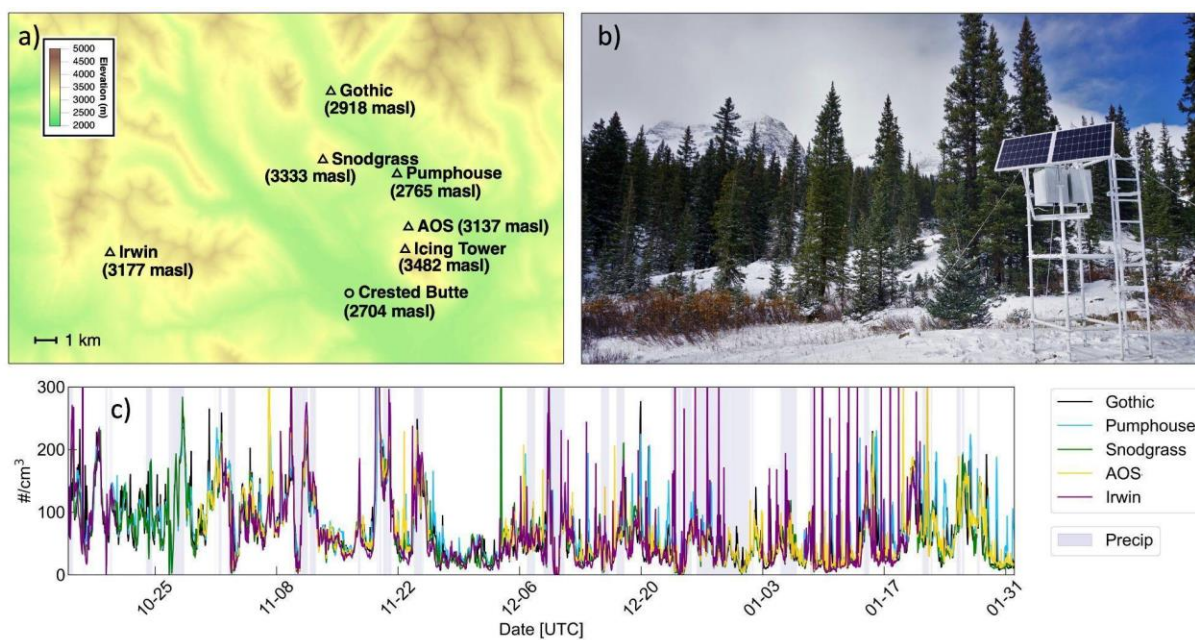


*Figure 8: a) Map of the SAIL-NET sites (triangles) along with the town of Crested Butte (circle), b) Example of the sixth site ('Irwin'), c) hourly averaged total number concentration between ~140 nm – 2 um (POPS instrument) from October 15, 2021 to January 31, 2022. The frequent wintertime spikes at the Irwin and AOS sites are due to snowmobile and snowcat*

*pollution. The precipitation (“Precip”) is from AMF-2 meteorology measurements and indicates which hours of the campaign experienced any measurable precipitation. The ‘Icing Tower’ site was set up late spring of 2022. The Snodgrass site is in the line of sight of the CSU X-band scanning radar.*

Initial investigation of aerosol spatial variability indicates remarkably consistent trends of aerosol number concentrations across all sites during the fall of 2021. Wintertime number concentrations still exhibit consistent trends from site to site but begin to show more variability from site to site (Figure 8c). Wintertime aerosol concentrations are heavily impacted by local pollution sources from snow machines, as can be seen at the Irwin and AOS sites (both of which sit next to high-use snow machine trails).

The AOS measurements collected to date, and the strong correlation between SAIL-NET and AOS data indicate that the aerosol data being collected, in conjunction with partnerships (see Section 8 for details), are broadly representative of ERW-scale atmospheric aerosol processes, so SAIL and SAIL-NET data are well-positioned to support science by providing information that helps address [SQ-2](#).

## **6. Aerosol-Cloud-Precipitation Interactions:**

Aerosols are known to strongly influence precipitation in complex terrain [[Givati and Rosenfeld, 2004](#); [Fan et al., 2014](#); [2017](#)] and previous work has found that that influence varies with terrain features such as mountain height and cross-section width [[Mühlbauer and Lohmann, 2006](#); [2008](#)]. Specifically, the spillover factor of precipitation (i.e., the precipitation ratio over the leeward to windward side) was found to be enhanced via increases in CCN [[Mühlbauer and Lohmann, 2006](#); [Saleeby et al., 2011](#); [Uin et al., 2019](#)] and INP [[Lin et al., 2022](#)]. Cloud phase – particularly the mixed-phase regime – and precipitation phase (i.e., rain or snow) could be very sensitive to INPs such as long-range transported dust and biological particles, leading to a large impact of aerosols on snow precipitation [[Creamean et al., 2013](#); [Fan et al., 2017](#)]. There are also coupled interactions between aerosols, precipitation, and circulation to consider: cloud microphysics feedback

to dynamics through aerosol-cloud interactions has been shown to change the mountain-valley circulation and enhance orographic mixed-phase clouds and precipitation [[Fan et al., 2017](#)]. For light-absorbing aerosols such as BC and BrC, aerosols can redistribute the moist static energy between the mountain and associated plain region and suppress mountain-valley circulation and reduce the precipitation in dry conditions [[Yang et al. 2016](#)]. There are outstanding uncertainties on these effects [[Choudhury et al., 2019](#)], and disagreements in the literature on whether aerosols enhance or suppress snowfall rates in mountains [[Borys et al., 2003](#); [Saleeby et al., 2011](#); [Fan et al., 2017](#)], maybe due to different mountain widths and heights, different meteorological conditions and physics parameterizations, etc. Therefore, aerosol-cloud-precipitation interactions over terrain need to be studied based on local terrain characteristics and considering typical meteorological conditions, which is one of the major goals for SAIL ([SO-4](#)).

The simultaneous, collocated measurements of CCN, INPs, precipitation, and thermodynamic conditions at S2 capture information on regional- and long-range transported aerosols, and also provide information to shed light on the disagreements in the literature of how aerosols impact and are impacted by precipitation. The INP data collected at SAIL provide particular insight into cold-season aerosol-cloud-precipitation interactions [[DeMott et al., 2010](#); [Hoose and Möhler, 2012](#); [Creamean et al., 2013](#)]. During SAIL, filter samples for offline measurement of INPs are being collected approximately every 3 days at the AOS following [Creamean et al. \[2022\]](#). Preliminary data are shown in [Figure 9](#). There are clear seasonal distinctions between fall/spring (higher concentrations) and winter (lower concentrations), which may be impacted by the wildfires in the fall of 2021 and the dusty spring of 2022, and, at least for September 2021, impacted by the local valley sources at M1 instead of S2. These results suggest that further measurements are needed to assess: 1) the INP seasonal cycle and investigate its phenomenology (i.e., why is there a significant seasonal cycle), 2) whether lower wintertime INP concentrations inhibit snowfall, 3) why INPs exhibit a non-log-linear relationship between above -15 °C in some months but not others [[Hill et al., 2016](#)], and 4) if the observations in 2021-2022 are representative of typical winters.

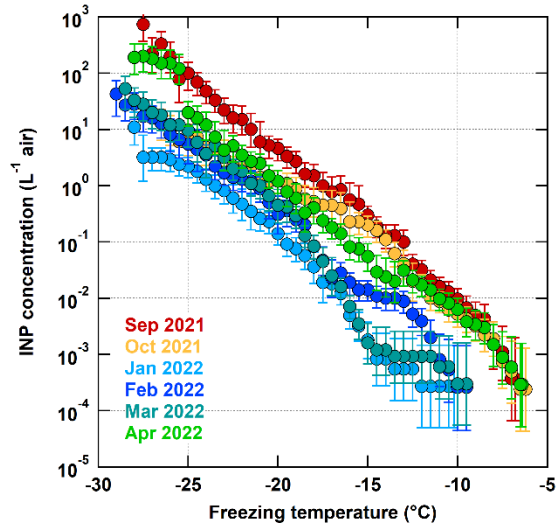


Figure 9: SAIL's preliminary cumulative [INP](#) spectra from filter samples collected during select months.

Preliminary data from the warm-season also indicate that the observations collected by SAIL provide a rich level of information on aerosol-cloud-precipitation interactions. [Figure 10](#) shows three precipitation events from May, 2022 that were associated with increased supermicron (particles with diameters  $\geq 1 \mu\text{m}$ ) aerosol events and winds from the south. Gas-phase carbon monoxide (CO) values do not exceed 125 ppbv, indicating the source of the particles is not likely anthropogenic pollution. BC measurements by the single particle soot photometer (SP2) also support this, as BC concentrations were below  $50 \mu\text{g m}^{-3}$ . The absorption angstrom exponent (AAE) for 470 nm / 660 nm indicated that the dominant absorbing species in the submicron (particles with diameters  $\leq 1 \mu\text{m}$ ) fraction was BC since the average AAE for the month was  $1.15 \pm 0.40$ , but that other absorbing species like brown carbon or absorbing dusts were likely present since  $\text{AAE} > 1$ . The single scattering albedo (SSA) average for the month at 450 nm was  $0.92 \pm 0.03$  for  $\text{PM}_{10}$  and  $0.93 \pm 0.02$  for  $\text{PM}_{2.5}$  indicating an overall presence of scattering particles.

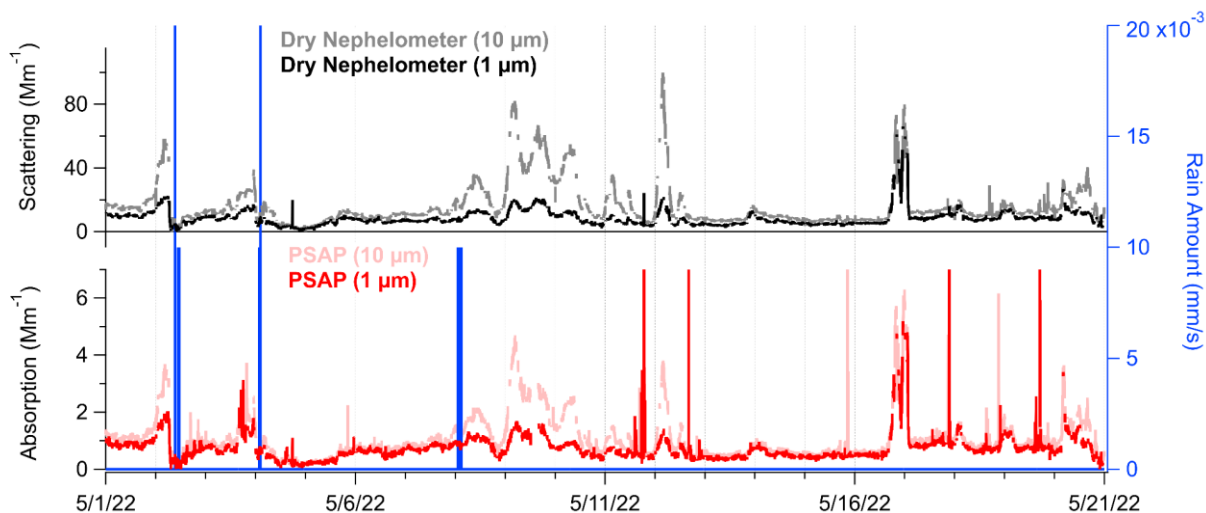


Figure 10: Particulate scattering and absorption coefficients as detected by the [NEPH](#) at 450 nm and [PSAP](#) at 470 nm in the AOS. Blue markers/lines represent precipitation events.

The first precipitation event on May 2 started at 09:15 UTC and was preceded by a particulate event of increased absorption and scattering that started the day before at 19:00 UTC on May 1 and continued to 06:30 UTC on May 2 with peak values at 06:15 UTC ([Figure 10](#)). Submicron number concentrations averaged 887 #/cc, and black carbon concentrations reached 55 ng/m<sup>3</sup> indicating there was likely some pollution that could be due to regional or long-range transport even though CO was below 115 ppbv. The second event occurred on May 4 and was similar to the first event: it was also preceded by a period of enhanced scattering and absorption that occurred with an average number concentration of 1083 #/cc, BC concentrations of ~42.2 ng m<sup>-3</sup> and CO < 125 ppbv. The third event occurred on May 8, preceding three days from May 8 - 10 of high particulate scattering and absorption coefficients where submicron number concentrations ranged from 400 to 1430 with an average concentration of 813 #/cc and CO was an average of 106 ± 4 ppbv. BC concentrations were not available.

A biomass burning event was observed from May 16 at 18:15 UTC to May 17 01:30 UTC. NOAA's High Resolution Rapid Refresh (HRRR)-Smoke model [[Ahmadov et al, 2017](#)] indicated the origin was from the Hermits Peak/Calf Canyon Wildfire in New Mexico,

approximately 300 km away. At SAIL, CO levels peaked at 193 ppbv, indicating combustion sources. Unlike the events associated with precipitation in early May, this event was dominated by particles in the submicron size range. Also, the TBS was deployed during this event. [Figure 11](#) shows the TBS vertical profiles that had two concentrated plumes at 2898 m and 2963 m in addition to elevated particle concentrations between 200 – 400 cm<sup>-3</sup> that were well-mixed within the boundary layer up to 3150 m during the second ascending branch of that TBS flight. The KAZR reflectivity profiles within the TBS flight window (bottom panel of Figure 11) indicates that the biomass burning aerosols appear to be interacting with clouds in this case.

The observations collected to date at SAIL indicate that there are evident aerosol-cloud-precipitation interactions which highlight mysteries on this subject that have yet to be resolved. SAIL will enable researchers to identify relationships between aerosol characteristics including both CCN and INPs and cloud properties such as cloud-water path, ice-water path, cloud phase, and precipitation for various meteorological conditions.

Associated process modeling studies (e.g., [Xu *et al*, 2023]) can focus on the intersection between aerosol regimes and synoptic/mesoscale conditions in the UCRB. These include long-range transported dust and biomass burning aerosols, secondary aerosol production, biogenic aerosols, and anthropogenic aerosols generated locally both from combustion and land-use activities as well as from cloud-seeding. SAIL and SAIL-NET data will be especially helpful for evaluating microphysics parameterizations to determine if they exhibit the sufficient level of complexity to capture quantitatively how the aerosol environment of the UCRB impacts clouds and precipitation. Considering the new version of the Energy Exascale Earth System Model (E3SM; [Golaz *et al*, 2022]) (v3; publicly available June 2023) will have a new cloud microphysics scheme, those data would be helpful to the evaluation of such parameterizations and aerosol-cloud interaction forcing for this new version of E3SM.

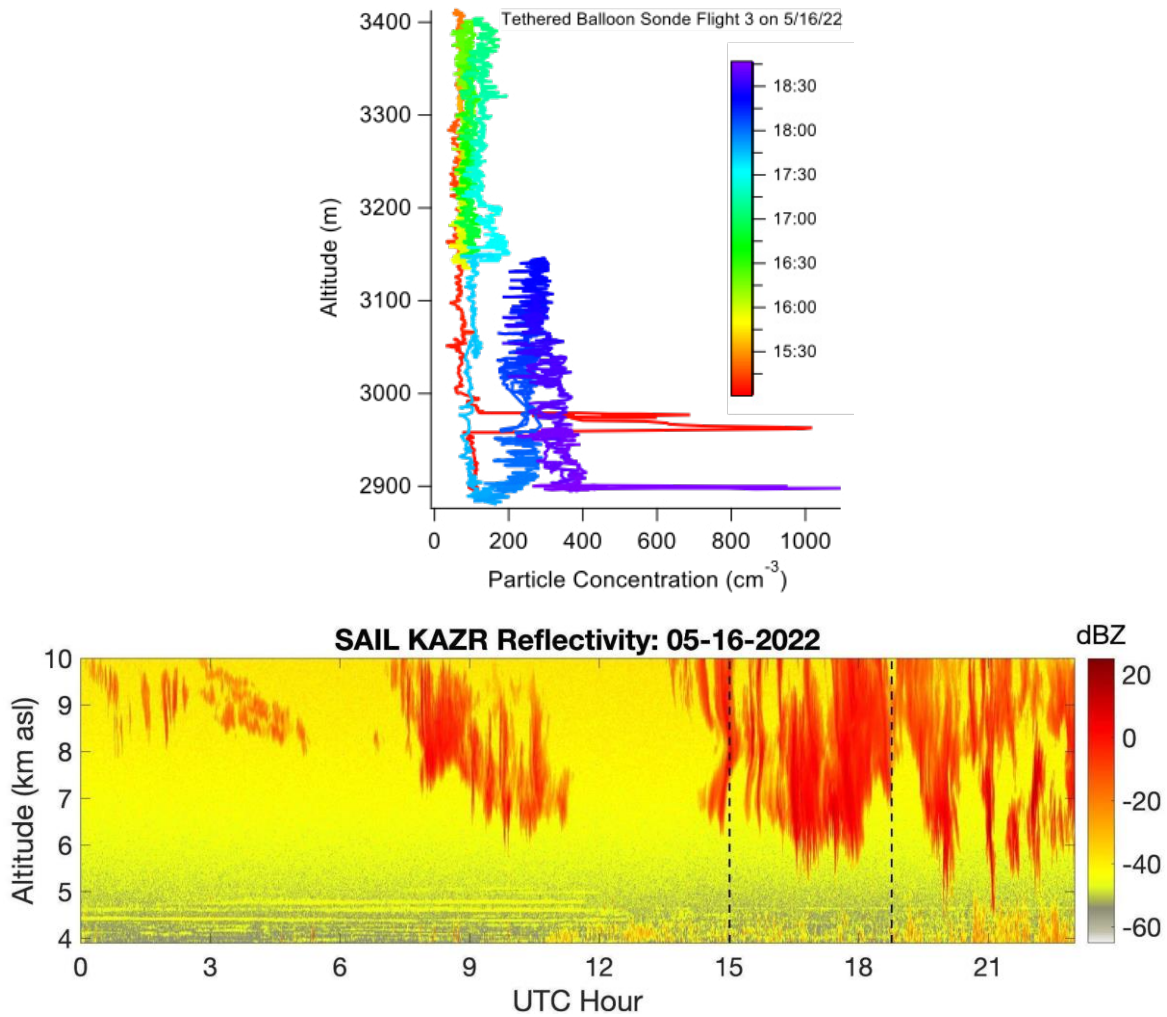


Figure 11: (Upper Panel) Particle number concentrations versus altitude measured by the POPS on the ARM TBS on May 16, 2022 between 15:01 UTC and 18:46 UTC. The colors represent the time the data was collected from the start of the TBS flight. (Lower Panel) Time-series of KAZR reflectivity profiles with TBS flight window denoted by dashed lines showing cloud particles.

## 7. Surface Energy Science:

In the high-altitude complex terrain of the ERW, the SEB varies dramatically across seasons. In the winter and spring, it exerts control on the evolution of the frozen surface state and local dynamics, and in the summer, it exerts control on both local and regional dynamics. Closing the SEB in snow-dominated environments has proven challenging, even

with collocated observations of shortwave and longwave radiation components, ground heat flux, and latent heat fluxes [[Helgason and Pomeroy, 2012](#)]. During the warm season, local radiative forcing becomes increasingly important for large-scale circulation, driving low-level flow that transports water vapor into the continental interior from the Gulf of California and Gulf of Mexico [[Adams and Comrie, 1997](#)]. Radiative fluxes in the Rockies are thus crucial for controlling regional-scale winds and precipitation in summer; these fluxes produce a column-integrated energy source (CIES) that is positive over all of North America in summer and is particularly strong over western orography. The poleward extent of North American monsoon rainfall is set by a balance between this net, continental-scale energy source and the advection of low-energy air from the cold, mid-latitude ocean [[Chou and Neelin, 2003](#); [Neelin, 2007](#); [Boos and Pascale, 2021](#)]. In spite of the motivation for developing SEB estimates from the watershed scale to the mountain range scale, the heterogeneity of the SEB terms (shortwave and longwave radiation, sensible and latent heat, and ground heat flux) in complex terrain led [Bales et al. \[2006\]](#) to pose the following open research question: “How do we represent and scale basin-wide energy balance in complex, heterogeneous terrain from sparse point measurements?”

Because it is completely infeasible to measure these fluxes everywhere all the time, physically-based models of SEB terms are necessary, so one of the areas of scientific advance for SAIL is to collect measurements across a wide range of surface and atmospheric conditions to test the robustness of such models, which have shown varying levels of skill in clear-sky and all-sky conditions [[Gubler et al, 2012](#)].

In response to this question, the SAIL campaign is addressing [SO-5](#) by developing a set of observations that can decompose and understand the primary controls on the terms of the seasonally-varying SEB. With such a result, researchers can evaluate the skill of radiative transfer models, for example, since these models are central to atmospheric and land-surface process models, and are the same or similar radiative transfer models are often used in Earth System Models.

The point measurements of surface upwelling and downwelling shortwave and longwave radiation and sensible and latent heat that SAIL is collecting, along with similar measurements collected by SPLASH, form a valley transect of SEB observations with different sky-view geometries where historical SNOTEL observations indicate that there are gradients in temperature, snowfall, and snowpack.

There have been and will be first-order effects on the SEB as the frozen surface conditions and snow impurities change seasonally, and also due to changing cloud cover throughout the SAIL campaign. This transect of data points provides a wide range of tests of radiative transfer models, and one of the key areas of scientific focus is the skill of such models in complex terrain.

A key feature of SAIL and SPLASH data is that they enable testing the real-world contributions of terrain to downwelling shortwave and longwave radiation. Specifically, they allow researchers to evaluate the magnitude and sign of the biases arising from the assumption that surface radiation can be calculated with a one-dimensional model and they allow for the determination of how those biases change seasonally. Three-dimensional terrain effects have been calculated [[Lee et al, 2015](#); [Feldman et al, 2022](#)] and found to be potentially significant sources of model error in complex terrain if they are omitted that lead to systematic biases in hydrological modeling. However, previously-published findings showing that terrain effects are significant for mountainous hydrology do not take into account the time-varying atmospheric and surface conditions. Clouds, aerosols, and heterogeneous frozen-surface conditions can all impact surface radiation, and SAIL data provide a large number of atmospheric and surface conditions to determine if unbiased radiative transfer modeling in complex terrain needs first to focus on terrain effects or the representations of clouds or aerosols. This is possible because ARM observations can support radiative closure studies (e.g., [[McFarlane et al, 2016](#)]) to provide a critical test of calculations of model error from terrain effects to ensure that surface radiation is calculated accurately and is not, through the simple omission of terrain effects, biasing hydrological modeling [[Feldman et al, 2022](#)].

## 8. **Partnerships:**

The SAIL campaign datastreams are augmented through a set of partnerships that bring additional resources, including both logistical support and additional observations. Each of these partners recognizes the importance of UCRB water resources but also have different goals and objectives for their work in the ERW.

First and foremost, the campaign maintains close ties to the DOE-sponsored Watershed Function Scientific Focus Area (SFA) [<https://watershed.lbl.gov> and Hubbard et al, 2018]. There are many facets to this partnership, but with respect to SAIL Science Objectives, the SFA provides additional precipitation observations, 1-2 lidar surveys per year of the spatial distribution of snow-water equivalent from the Airborne Snow Observatory (ASO) [[Painter et al, 2016](#)] across the entire ERW, detailed surface vegetation observations collected by NEON lidar also across the entire ERW [[Goulden et al, 2020](#)], additional eddy covariance measurements [[Ryken et al, 2022](#)], additional aerosol measurements [[Christensen et al, 2015](#); [Asher et al, 2018](#)], and a wide-ranging set of knowledge, perspectives, and modeling expertise from the surface and subsurface hydrologists that the SFA supports [[Hubbard et al, 2018](#); [2020](#)]. The SFA also provides direct measurements of groundwater and streamflow, thereby achieving simultaneous atmosphere-through-bedrock observations to advance holistic watershed function understanding.

Through the SFA, there are additional measurements of the snowpack in the ERW that directly support [SO-2](#). During the SAIL campaign, ASO surveyed the SAIL study area in 2022 (as shown in [Figure 12](#)), and also plans to measure in 2023. These observations of 3-meter snow depth, surface hyperspectral reflectance, and surface skin temperature are complemented by daily satellite-based maps of snow fraction, snow albedo, snow grain size, and dust radiative forcing on snow with MODIS [[Painter et al., 2009](#); [Painter et al., 2012](#); [Dozier et al., 2008](#); [Rittger et al., 2021](#)], which are presented in near-real time via Snow Today (<https://nsidc.org/snow-today>) at the National Snow and Ice Data Center.

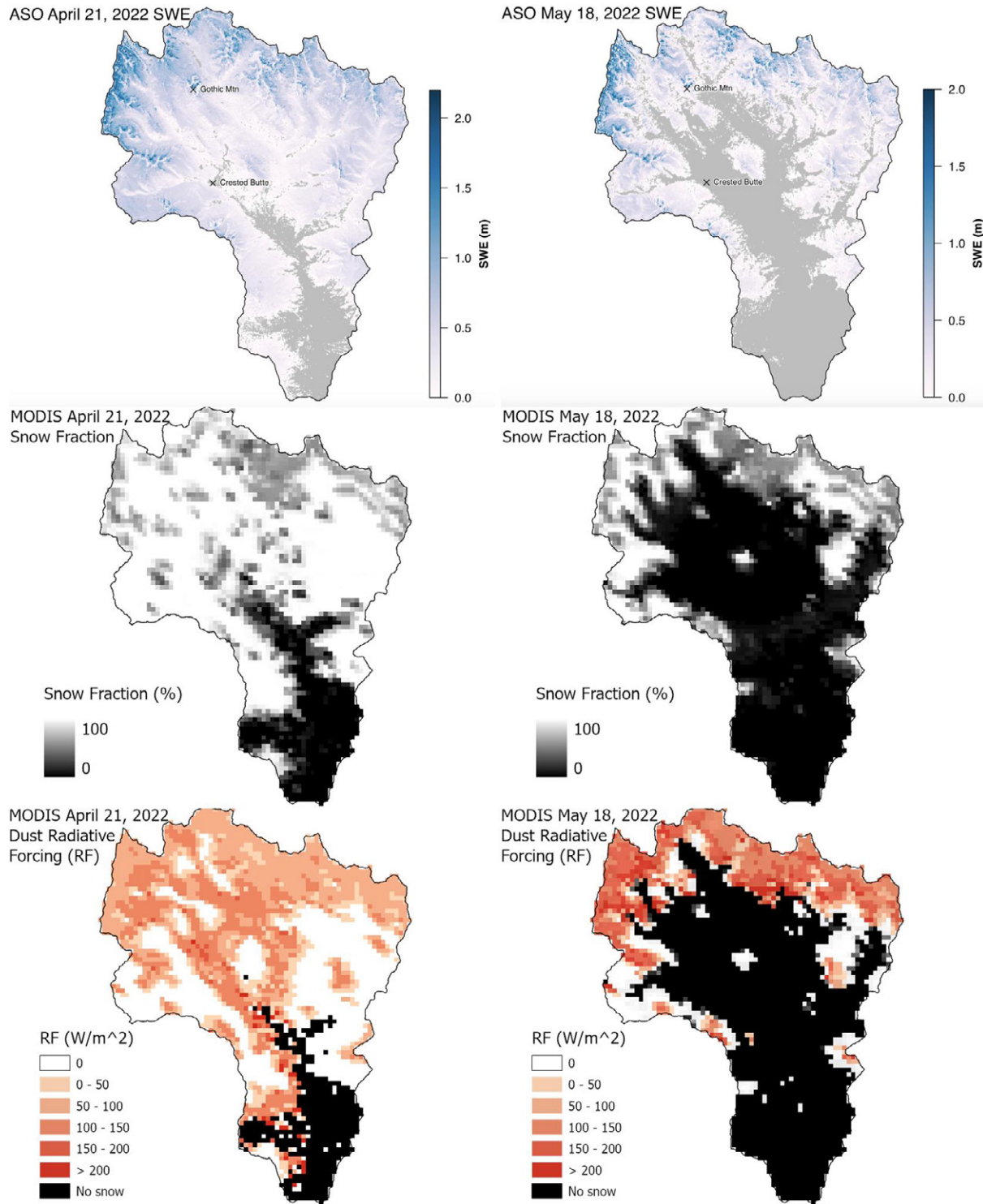


Figure 12: (top row) ASO SWE observational products over the ERW, (middle row) MODIS snow fraction, and (bottom row) MODIS dust radiative forcing (over non-forested areas) on (left column) April 21, 2022 and (right column) May 18, 2022. MODIS data are from MODSCAG and MODDRFS.

Additional partnerships facilitated with the Watershed Function SFA include ongoing snowpit measurements [[Skiles et al. 2015](#); [2016](#); [2017](#)] at Gothic to characterize dust deposition on the snowpack across the winter, and paired forest-open meteorological stations and intensive snowpit surveys on Snodgrass Mountain.

Second, the Rocky Mountain Biological Laboratory (RMBL) serves as the primary host for SAIL instrumentation. Their technical and logistical support has enabled the deployment of SAIL to its M1, S2, and S3 locations. They also have collected a wide range of long-duration observations that are continuing through the SAIL campaign and provide context to its observations. These include, but are not limited to, decades of continuous vegetation, weather [[Inouye et al. 2000](#)] and aerosol deposition [[Clarke et al. 1997](#)] measurements at Gothic, as well as, more recently, biweekly aerial surveys of a  $\sim 2$  km<sup>2</sup> area encompassing M1 to collect vegetation and snow cover information [[Breckheimer et al. 2021](#)].

Third, the Study of Precipitation, the Lower Atmosphere and Surface for Hydrometeorology (SPLASH) campaign is supported by National Oceanic and Atmospheric Administration (NOAA) and has concurrently deployed instrumentation to collect information on dozens of atmospheric quantities that are the same, similar, or complementary to SAIL observations. SPLASH started in September 2021 and will extend through September 2023, thereby overlapping nearly completely with the SAIL campaign. SPLASH has deployed instruments to four separate locations across the ERW to span north-south gradients in surface energy and mass budgets. An eddy-covariance and surface meteorological system has been deployed to the Avery Picnic site, and eddy-covariance, precipitation, and radiation measurements have been deployed to the S3 site, while eddy-covariance, precipitation, radiation, and boundary layer profiling measurements have been deployed to the Brush Creek site, which is 3 km south of S2 and at a location that receives far more radiation and far less snow than the other SAIL sites. Surface meteorological sensors, and additional boundary layer profilers have been deployed to the Roaring Judy Fish Hatchery, which is 20 km south of S2. In addition, SPLASH has supported the

deployment of crewed and uncrewed aircraft systems to capture information on surface state, including surface reflectivity (albedo), snow cover, soil moisture, and SWE. SPLASH data are available at <https://psl.noaa.gov/splash/> and greatly augment SAIL's precipitation observations and provide 3 additional radiometric and surface energy budget observations that span the north-south gradient of precipitation, temperature, and radiation.

*Table 3: Guest Instruments Deployed to SAIL as of March 8, 2023.*

<i>Campaign Name</i>	<i>Dates</i>	<i>Instrument(s)</i>	<i>Purpose</i>	<i>Location</i>	<i>Lead Scientist</i>
<i>SAILCAIVIMT</i>	<i>9/21 - 6/23</i>	<i>Aerosol PSDs, CCN concentrations, and INP throughout ERW.</i>	<i>Characterize aerosol spatial variability and its causes and implications in ERW.</i>	<i>M1, S2 and 4 other locations</i>	<i>Ezra Levin (Handix)</i>
<i>CPA</i>	<i>9/21 - 6/23</i>	<i>Size- and Time-resolved Aerosol Collector</i>	<i>Determine aerosol size-resolved chemical composition</i>	<i>S2</i>	<i>Swarup China (PNNL)</i>
<i>SAILAEROSSAMPL</i>	<i>10/21 - 6/23</i>	<i>Aerosol particle collection with chemical imaging and molecular characterization</i>	<i>Establish a relationship between the composition of aerosol particles and their atmospheric impacts</i>	<i>S2</i>	<i>Alex Laskin (Purdue U.)</i>
<i>TWSTSAIL</i>	<i>10/21 - 6/23</i>	<i>Cloud optical depth, droplet effective radius, and thermodynamic phase</i>	<i>Validate Aerodyne's cloud property sensors in high-altitude complex terrain</i>	<i>M1</i>	<i>Stephen Jones (Aerodyne)</i>
<i>WFSDB</i>	<i>12/21 - 10/25</i>	<i>Citizens Band Radio Service</i>	<i>To develop a high-bandwidth 5G wireless network for connecting field</i>	<i>S2 (hub of network)</i>	<i>Andrew Wiedlea (LBNL)</i>

			<i>instruments.</i>		
<i>SSB</i>	4/22 - 6/23	<i>Supermicron aerosol and bioaerosols</i>	<i>Determine if supermicron bioaerosols influence aerosol processes, aerosol-cloud interactions, and the hydrological cycle</i>	<i>S2</i>	<i>Allison Aiken (LANL)</i>
<i>SAILVAPS</i>	4/22 - 11/22	<i>Time-resolved vertical profiles of CCN and INPs</i>	<i>Assess vertical gradients in aerosols on TBS</i>	<i>MI</i>	<i>Russell Perkins (CSU)</i>
<i>PBAS</i>	5/22 - 7/22	<i>Vertical profiles of bioaerosols</i>	<i>Assess vertical gradients in bioaerosols on TBS</i>	<i>MI</i>	<i>Maria Zawadowicz (BNL)</i>
<i>SAIL-AVP</i>	9/22 - 4/23	<i>Vertical profiles of CCN and INPs</i>	<i>Assess vertical gradients in aerosols on TBS</i>	<i>PH</i>	<i>Allison Aiken (LANL)</i>
<i>SAIL-ISO</i>	6/22 - 6/23	<i>Stable isotopic composition of water vapor</i>	<i>Collect information on sources and sinks of atmospheric water vapor</i>	<i>MI</i>	<i>Joseph Galewsky (U. New Mexico)</i>
<i>SAILTOBS</i>	9/22 - 6/23	<i>Snowflake cameras and acoustic mass-flux sensors</i>	<i>Observe mixed-phase and frozen hydrometeors in winter</i>	<i>MI, S3</i>	<i>Aaron Kennedy (U. North Dakota)</i>
<i>SAILCORSIPP</i>	9/22- 6/23	<i>W-band scanning radar and snowflake camera</i>	<i>Characterization of orographically induced riming</i>	<i>MI</i>	<i>Max Maahn (U. Leipzig)</i>
<i>SOS</i>	9/22 - 6/23	<i>Integrated Surface Flux System [UCAR/NCAR, 1990]</i>	<i>Directly measure sublimation from snowpack and blowing snow.</i>	<i>S3</i>	<i>Jessica Lundquist (U. Washington)</i>

Fourth, the SAIL campaign maintains close ties with a campaign supported by the National Science Foundation called Sublimation of Snow (SOS). This campaign directly supports SAIL's [SO-2](#) that pertains to snow sublimation and wind redistribution. As part of SOS, the Earth Observing Laboratory deployed four flux towers, each with a terrestrial lidar scanner at Kettle Ponds to measure the sublimation of the snowpack directly at that site. The SOS project will use SAIL data to understand the larger-scale mountain-valley turbulence to specifically measure how sublimation at a point relates to valley scale circulation and water vapor fluxes through the atmosphere.

Fifth, SAIL interfaces with a number of federal, state, and local water monitoring and forecasting agencies, including the USGS Next Generation Water Observing System (NGWOS), the US Bureau of Reclamation (USBR), and the Upper Gunnison Water Conservancy District. Collaborative efforts include leveraging SAIL precipitation retrievals and energy balance estimates for improved water supply forecasting, as well as model development and verification for USBR led anthropogenic cloud-seeding (weather modification) efforts.

Finally, SAIL has a built-in capability that enables community research. ARM is a national user facility, and therefore has an established process for supporting guest instruments, including by providing ongoing logistical support for such instrumentation. Numerous guest instruments have already been deployed, as listed in [Table 3](#), and interested groups are encouraged to submit proposals for such support.

## 9. Summary and Discussion

Given the importance of the watersheds of the UCRB to ecosystems and societies in the West, the integrated understanding and prediction of these systems is paramount, as highlighted in the Department of Energy's interest in Integrated Mountainous Hydroclimate [*U.S. DOE*, 2022]. Nevertheless, these systems are poorly sampled or lack observations sufficient to constrain model development, and as such there is no clear path towards substantive improvements in understanding and prediction of these systems

[[Vano et al, 2014](#)]. SAIL seeks to make substantive contributions to mountainous hydrology in the UCRB through the simultaneous collection of atmospheric, surface and subsurface observations. The goal is to determine, in the UCRB, what is the minimum but sufficient amount of atmospheric and land-atmosphere interaction process information needed to develop unbiased seasonal estimates of the surface energy and water budgets.

To achieve this goal, SAIL is multi-faceted out of necessity: there are many simultaneously occurring, interconnected processes in the atmosphere, land-surface, and sub-surface that impact mountainous hydrology. Because the UCRB is an area with significant, large, multiscale gradients and first-order spatial and temporal heterogeneity in mountainous hydrology, it is infeasible to develop observational constraints of the dominant hydrological processes at all locations across the basin at all times.

One of the distinguishing features of SAIL is that it features multiple simultaneous measurements of the atmosphere collocated with multiple simultaneous measurements collected by its partners. These are useful for developing multivariate observational analyses of processes, especially for point observations where questions of representativeness must be addressed in the face of substantial spatial heterogeneity. It is the combination of multiple datastreams, capturing diel, synoptic, seasonal and interannual variability that enable a cutting-edge scientific exploration of the processes of interest for SAIL.

To that end, while SAIL, with a duration of 21 months, is undersampling interannual hydrological variability in the UCRB, SAIL's approach is designed to aid the scientific community by using a large number of simultaneous, independent datastreams to interrogate major hydrological process in the ERW. It is thereby establishing the level of required observational detail to advance the predictive understanding of mountainous hydrology beyond the ERW and across the UCRB. Furthermore, because measurements from the Watershed Function SFA including airborne snow surveys and from RMBL of surface precipitation both preceded (in the case of RMBL, by decades) and will succeed

SAIL and thereby capture interannual hydrological variability, the information produced from the SAIL data can show where and when Watershed Function SFA and RMBL observations are skillful and representative of larger features of the ERW and advance hydrology research across that longer envelope.

Because SAIL covers two autumns, two winters, two springs, and one summer, it also enables the collection of data, interim analysis, and the development of hypotheses regarding dataset features that vary seasonally and the testing of those hypotheses with data during the second half of the SAIL campaign. The formulation and testing of these hypotheses can be very useful for answering SAIL's overarching science question because they focus on forming generalizations from the data when not all of it has been collected.

The cold-season snowpack accumulation at the SNOTEL stations in the ERW for WY22 was within 5% of the 1990-2020 median, but the spring experienced more long-range dust transport and stronger winds than average in the spring of 2022. Meanwhile, the summer monsoon was very strong, with dozens of thunderstorms experienced by SAIL.

Nevertheless, the meteorological events of SAIL's 21 months of data collection enable atmospheric, surface, and sub-surface process analyses, though interannual variability in precipitation and aerosols, may be under-sampled during SAIL's 21 months of data collection given the persistent La Niña conditions in WY21 and WY22 and limited number of western states wildfires. Follow-on observations that build off of SAIL in the ERW and across the UCRB, should they be available, will create more confidence that the findings from SAIL are relevant and representative of atmosphere-through-bedrock interactions across the UCRB. Precipitation radar, distributed aerosol collection, and sensing that leverage the wireless network capabilities that SAIL enabled, are priority observations for the ERW and UCRB after the completion of the SAIL campaign. These can establish a baseline monitoring network to contextualize SAIL observations so that they can be used as a starting-off point to catalyze periodic, intensive follow-up observations to ensure that the mountainous hydrology scientific community's needs for comprehensive observations,

which engendered SAIL in the first place, are not going unfulfilled beyond the end date of the SAIL campaign.

Connections to modeling activities are critical to SAIL's contributions to hydrology, since new and/or improved process models will be required to extend the scientific findings from SAIL to larger basins to support future water resource predictions. To date, there are ongoing efforts to support SAIL through concurrent simulations of the Weather Research and Forecasting (WRF) model [[Rudisill et al, 2022](#); [Xu et al, 2023](#)], variable-resolution Earth System Modeling [[Rhoades et al; 2018a,b](#)], and surface/subsurface process modeling [[Maina et al, 2022](#)]. Ultimately, process models serve as an important bridge to developing a sufficient process representation competency in Earth System Models.

Finally, given the scope of the campaign, there is a substantial amount of information in the data being collected that awaits analysis from the larger scientific community.

**Acknowledgements:**

This work was supported by the U.S. Department of Energy, Office of Science, Office of Biological and Environmental Research and the Atmospheric System Research under U.S. Department of Energy Contract No. DE-AC02-05CH11231. This research used resources of the National Energy Research Scientific Computing Center, a DOE Office of Science User Facility supported by the Office of Science of the U.S. Department of Energy under that same contract.

**Data Availability:**

All SAIL data used in this work is freely available at the ARM Data Discovery <https://adc.arm.gov/discovery/>. ASO data is freely available at <https://data.airbornesnowobservatories.com/> and MODIS snow cover and radiative forcing data are freely available at [https://nsidc.org/snow-today/data\\_request#no-back](https://nsidc.org/snow-today/data_request#no-back).

## **References:**

Abatzoglou, J., et al, (2021) California's Missing Forecast Flows in Spring 2021 – Challenges for seasonal flow forecasting, *California Water Blog Posting on July 18, 2021*, <https://californiawaterblog.com/2021/07/18/californias-missing-forecast-flows-in-spring-2021-challenges-for-seasonal-flow-forecasting/>.

Adams, D. K., & Comrie, A. C. (1997). The North American Monsoon. *Bull. Amer. Meteor. Soc.*, **78**, 2197–2213, doi:[10.1175/1520-0477\(1997\)078<2197:TNAM>2.0.CO;2](https://doi.org/10.1175/1520-0477(1997)078<2197:TNAM>2.0.CO;2)

Ahmadov, R. et al., (2017), Using VIIRS fire radiative power data to simulate biomass burning emissions, plume rise and smoke transport in a real-time air quality modeling system, *2017 IEEE International Geoscience and Remote Sensing Symposium (IGARSS)*, 2806-2808, doi: [10.1109/IGARSS.2017.8127581](https://doi.org/10.1109/IGARSS.2017.8127581).

Asher, E. C., et al. (2018). The transport of Asian dust and combustion aerosols and associated ozone to North America as observed from a mountaintop monitoring site in the California Coast Range. *J. Geophys. Res. Atmos.*, **123**, 5667-5680. doi: [10.1029/2017JD028075](https://doi.org/10.1029/2017JD028075).

Bailey, K., et al. (2021) Western Water Assessment Water Year 2021 Summary, <https://wwa.colorado.edu/resources/intermountain-west-climate-dashboard/briefing/water-year-2021-summary>.

Bales, R. C., et al. (2006), Mountain hydrology of the western United States, *Water Resour. Res.*, **42**, W08432, doi:[10.1029/2005WR004387](https://doi.org/10.1029/2005WR004387).

Barros, A. & M. Arulraj (2020) Remote Sensing of Orographic Precipitation, In: Levizzani, V., Kidd, C., Kirschbaum, D., Kummerow, C., Nakamura, K., Turk, F. (eds) *Satellite Precipitation*

Measurement. *Adv. Clim. Chang. Res.*, **69**. Springer, Cham. doi: [doi:10.1007/978-3-030-35798-6\\_6](https://doi.org/10.1007/978-3-030-35798-6_6).

Berghuijs, W. R., et al. (2014), A precipitation shift from snow towards rain leads to a decrease in streamflow. *Nat. Clim. Change*, **4**, 583-586, doi:[10.1038/nclimate2246](https://doi.org/10.1038/nclimate2246).

Bond, T. C., et al. (2013), Bounding the role of black carbon in the climate system: A scientific assessment, *J. Geophys. Res. Atmos.*, **118**, 5380–5552, doi:[10.1002/jgrd.50171](https://doi.org/10.1002/jgrd.50171).

Boos, W., and S. Pascale (2021) Mechanical forcing of the North American monsoon by orography. *Nature*, **599**, 611–615, doi:[10.1038/s41586-021-03978-2](https://doi.org/10.1038/s41586-021-03978-2).

Börk, K., et al. (2022) Adapting to 4 Degrees C World, *Environmental Law Reporter*, **52**, 10211, <https://www.elr.info/sites/default/files/files-general/52.10211.pdf>.

Borys, R.D., et al. (2003). Mountaintop and radar measurements of anthropogenic aerosol effects on snow growth and snowfall rate. *Geophys. Res. Lett.*, **30**(10), doi:[10.1029/2002GL016855](https://doi.org/10.1029/2002GL016855).

Breckheimer, I., et al. (2021) Integrative Remote Sensing to Promote Environmental Discovery: The RMBL Spatial Data Platform, AGU Fall Meeting 2021, held in New Orleans, LA, 13-17 December 2021, id. GC22E-05.

Bruce, B.W., 2012, WaterSMART—The Colorado River Basin focus-area study: U.S. Geological Survey Fact Sheet 2012–3114, 6 p.

Christensen, J. N., et al (2015) Unraveling the sources of ground level ozone in the Intermountain Western United States using Pb isotopes, *Sci. Total Environ.*, 530-531, 519-525, doi:[10.1016/j.scitotenv.2015.04.054](https://doi.org/10.1016/j.scitotenv.2015.04.054).

Chou, C., & Neelin, J. D. (2003). Mechanisms limiting the northward extent of the northern summer monsoons over North America, Asia, and Africa. *J. Climate*, **16**, 406–425, doi:[10.1175/1520-0442\(2003\)016<0406:MLTNEO>2.0.CO;2](https://doi.org/10.1175/1520-0442(2003)016<0406:MLTNEO>2.0.CO;2)

Choudhury, G., et al. (2019). Aerosol-orography-precipitation – A critical assessment, *Atmos. Environ.*, 214, doi: [10.1016/j.atmosenv.2019.116831](https://doi.org/10.1016/j.atmosenv.2019.116831).

Clark, M. P., et al. (2015a), A unified approach for process-based hydrologic modeling: 1. Modeling concept, *Water Resour. Res.*, **51**, 2498–2514, doi:[10.1002/2015WR017198](https://doi.org/10.1002/2015WR017198).

Clark, M. P. et al. (2015b), A unified approach for process-based hydrologic modeling: 2. Model implementation and case studies, *Water Resour. Res.*, **51**, 2515–2542, doi: [10.1002/2015WR017200](https://doi.org/10.1002/2015WR017200).

Clarke, J.F., et al (1997) Dry deposition calculations for the clean air status and trends network, *Atmos. Environ.*, **31**(21), 3667-3678, doi: [10.1016/S1352-2310\(97\)00141-6](https://doi.org/10.1016/S1352-2310(97)00141-6).

Collis, S., et al, (2018), ARM: Corrected Moments in Antenna Coordinates, Version 2 (CMAC2), *U.S. DOE ARM Data Center*, doi:[10.5439/1855341](https://doi.org/10.5439/1855341).

Creamean, J. M., et al, (2022) Ice Nucleation Spectrometer (INS) Instrument Handbook, DOE/SC-ARM-TR-278, [https://www.arm.gov/publications/tech\\_reports/handbooks/doe-sc-arm-tr-278.pdf](https://www.arm.gov/publications/tech_reports/handbooks/doe-sc-arm-tr-278.pdf).

Creamean, J. M., et al., (2013) Dust and Biological Aerosols from the Sahara and Asia Influence Precipitation in the Western U.S. *Science*, **339**, 1572-1578, doi: [10.1126/science.1227279](https://doi.org/10.1126/science.1227279).

de Boer, G., et al. (2023) Supporting Advancement in Weather and Water Prediction: The SPLASH Campaign. *Bull. Amer. Meteor. Soc.*, (Submitted).

DeMott, P.J., et al, (2010) Predicting global atmospheric ice nuclei distributions and their impacts on climate, *Proc. Natl. Acad. Sci. U.S.A.*, **107**(25), 11217-11222, doi:[10.1073/pnas.0910818107](https://doi.org/10.1073/pnas.0910818107).

Dexheimer, D., et al., (2019), Evaluation of ARM tethered-balloon system instrumentation for supercooled liquid water and distributed temperature sensing in mixed-phase Arctic clouds, *Atmos. Meas. Tech.*, **12**, 6845-6864, doi: [10.5194/amt-12-6845-2019](https://doi.org/10.5194/amt-12-6845-2019).

Dozier, J. et al. (2008), Time–space continuity of daily maps of fractional snow cover and albedo from MODIS, *Adv. Water Resour.*, **31**(11), 1515-1526, doi: [10.1016/j.advwatres.2008.08.011](https://doi.org/10.1016/j.advwatres.2008.08.011).

Fan, J., et al. (2014), Aerosol impacts on California winter clouds and precipitation during CalWater 2011: local pollution versus long-range transported dust, *Atmos. Chem. Phys.*, **14**, 81–101, doi:[10.5194/acp-14-81-2014](https://doi.org/10.5194/acp-14-81-2014).

Fan, J., et al. (2015), Substantial contribution of anthropogenic air pollution to catastrophic floods in Southwest China. *Geophys. Res. Lett.*, **42**(14), 6066-6075, doi:[10.1002/2015GL064479](https://doi.org/10.1002/2015GL064479).

Fan, J., et al. (2017), Effects of cloud condensation nuclei and ice nucleating particles on precipitation processes and supercooled liquid in mixed-phase orographic clouds, *Atmos. Chem. Phys.*, **17**, 1017-1035, doi:[10.5194/acp-17-1017-2017](https://doi.org/10.5194/acp-17-1017-2017).

Fassnacht, S.R. (2021) Snow can disappear straight into the atmosphere in hot, dry weather, *The Conversation*, <https://theconversation.com/snow-can-disappear-straight-into-the-atmosphere-in-hot-dry-weather-162910>.

Feldman, D.R., et al. (2022), Three-dimensional Surface Downwelling Longwave Radiation Effects in the Upper Colorado River Basin, *Geophys. Res. Lett.*, **49**, e2021GL094605, doi: [10.1029/2021GL094605](https://doi.org/10.1029/2021GL094605).

Flanner, M. G., et al. (2009). Springtime warming and reduced snow cover from carbonaceous particles, *Atmos. Chem. Phys.*, **9**, 2481-2497, doi:[10.5194/acp-9-2481-2009](https://doi.org/10.5194/acp-9-2481-2009).

Frei, C. and Schär, C. (1998), A precipitation climatology of the Alps from high-resolution rain-gauge observations. *Int. J. Climatol.*, **18**, 873-900. doi:[10.1002/\(SICI\)1097-0088\(19980630\)18:8<873::AID-JOC255>3.0.CO;2-9](https://doi.org/10.1002/(SICI)1097-0088(19980630)18:8<873::AID-JOC255>3.0.CO;2-9).

Gangopadhyay, S., et al. (2022). Tree rings reveal unmatched 2nd century drought in the Colorado River Basin. *Geophys. Res. Lett.*, **49**, e2022GL098781. doi: [10.1029/2022GL098781](https://doi.org/10.1029/2022GL098781).

Gerlak, A.K., et al. (2021), Knowledge governance and learning: Examining challenges and opportunities in the Colorado River basin, *Environ. Sci. Policy*, **125**, 219-230, doi: [10.1016/j.envsci.2021.08.026](https://doi.org/10.1016/j.envsci.2021.08.026).

Givati, A. and D. Rosenfeld (2004) Quantifying Precipitation Suppression Due to Air Pollution, *J. Appl. Meteorol. Climatol.*, **43**(7), 1038-1056, doi: [10.1175/1520-0450\(2004\)043<1038:QPSDTA>2.0.CO;2](https://doi.org/10.1175/1520-0450(2004)043<1038:QPSDTA>2.0.CO;2).

Goulden, Tristan, et al. *NEON AOP Survey of Upper East River CO Watersheds: LAZ Files, LiDAR Surface Elevation, Terrain Elevation, and Canopy Height Rasters*. United States: N. p., 2020. Web. doi:10.15485/1617203.

Golaz, J.-C., et al. (2022). The DOE E3SM Model version 2: Overview of the physical model and initial model evaluation. *J. Adv. Model. Earth Syst.*, **14**, e2022MS003156. doi: [10.1029/2022MS003156](https://doi.org/10.1029/2022MS003156)

Groot Zwaaftink, C. D., et al. (2013). Seasonal simulation of drifting snow sublimation in Alpine terrain. *Water Resour. Res.*, **49**, 1581–1590. doi: [10.1002/wrcr.20137](https://doi.org/10.1002/wrcr.20137)

Gubler, S., S. Gruber, & R.S. Purves (2012) Uncertainties of parameterized surface downward clear-sky shortwave and all-sky longwave radiation, *Atmos. Chem. Phys.*, **12**(11), doi: 10.5194/acp-12-5077-2012.

Guntupally, K. et al. (2021) Enabling modern data discovery for atmospheric measurements. *Earth Sci. Inform.*, **14**, 1487-1502, doi: [10.1007/s12145-021-00635-0](https://doi.org/10.1007/s12145-021-00635-0).

Hamlet, A. F., et al. (2007), Twentieth-century trends in runoff, evapotranspiration, and soil moisture in the western United States. *J. Climate*, **20**, 1468-1486, doi:[10.1175/JCLI4051.1](https://doi.org/10.1175/JCLI4051.1).

Hansen, J., and L. Nazarenko (2004) Soot climate forcing via snow and ice albedos. *Proc. Natl. Acad. Sci. U.S.A.*, **101**, 423-428, doi:[10.1073/pnas.2237157100](https://doi.org/10.1073/pnas.2237157100).

Helgason, W. and J. Pomeroy, (2012) Problems Closing the Energy Balance over a Homogeneous Snow Cover during Midwinter. *J. Hydromet.*, **13**, 557–572, doi:[10.1175/JHM-D-11-0135.1](https://doi.org/10.1175/JHM-D-11-0135.1).

Henn, B., et al. (2016). Spatiotemporal patterns of precipitation inferred from streamflow observations across the Sierra Nevada mountain range. *J. Hydrol.*, doi:[10.1016/j.jhydrol.2016.08.009](https://doi.org/10.1016/j.jhydrol.2016.08.009).

Henn, B., et al. (2018). An assessment of differences in gridded precipitation datasets in complex terrain. *J. Hydrol.*, **556**, 1205-1219, doi: [10.1016/j.jhydrol.2017.03.008](https://doi.org/10.1016/j.jhydrol.2017.03.008).

Hill, T. C. J., et al, (2016) Sources of organic ice nucleating particles in soils. *Atmos. Chem. Phys.*, **16**, 7195-7211, doi:[10.5194/acp-16-7195-2016](https://doi.org/10.5194/acp-16-7195-2016).

Hood, E., et al. (1999), Sublimation from a seasonal snowpack at a continental, mid-latitude alpine site. *Hydrol. Process.*, **13**: 1781-1797, doi: [10.1002/\(SICI\)1099-1085\(199909\)13:12/13<1781::AID-HYP860>3.0.CO;2-C](https://doi.org/10.1002/(SICI)1099-1085(199909)13:12/13<1781::AID-HYP860>3.0.CO;2-C).

Hoose, C., and O. Möhler, (2012) Heterogeneous ice nucleation on atmospheric aerosols: a review of results from laboratory experiments. *Atmos. Chem. Phys.*, **12**, 9817-9854, doi: [10.5194/acp-12-9817-2012](https://doi.org/10.5194/acp-12-9817-2012).

Houze, R. A. (2012), Orographic effects on precipitating clouds, *Rev. Geophys.*, **50**, RG1001, doi:[10.1029/2011RG000365](https://doi.org/10.1029/2011RG000365).

Hubbard, SS, et al. (2018) The East River, Colorado, Watershed: A Mountainous Community Testbed for Improving Predictive Understanding of Multiscale Hydrological–Biogeochemical Dynamics, *Vadose Zone Journal*, **17**, 1-25 180061, doi: [10.2136/vzj2018.03.0061](https://doi.org/10.2136/vzj2018.03.0061).

Hubbard, SS, et al. (2020) Emerging technologies and radical collaboration to advance predictive understanding of watershed hydrobiogeochemistry. *Hydrol. Process.*, **34**, 3175–3182, doi: [10.1002/hyp.13807](https://doi.org/10.1002/hyp.13807).

Inouye, D., et al. (2000) Climate change is affecting altitudinal migrants and hibernating species, *Proc. Natl. Acad. Sci. U.S.A.*, **97**(4), 1630-1633, doi: [10.1073/pnas.97.4.1630](https://doi.org/10.1073/pnas.97.4.1630).

James, T, et al. (2014) The economic importance of the Colorado River to the basin region. *Final Rep., L. William Seidman Research Institute, Arizona State University*, 54, <https://businessforwater.org/wp-content/uploads/2016/12/PTF-Final-121814.pdf>.

Kaspari, S. D., et al. (2011), Recent increase in black carbon concentrations from a Mt. Everest ice core spanning 1860–2000 AD, *Geophys. Res. Lett.*, **38**, L04703, doi:[10.1029/2010GL046096](https://doi.org/10.1029/2010GL046096).

Laskin, A., et al. (2015) Chemistry of Atmospheric Brown Carbon, *Chem. Rev.* **115**, 10, 4335–4382, doi:[10.1021/cr5006167](https://doi.org/10.1021/cr5006167).

Lee, W.-L., et al, (2015), A global model simulation for 3-D radiative transfer impact on surface hydrology over the Sierra Nevada and Rocky Mountains, *Atmos. Chem. Phys.*, **15**, 5405-5413, doi:[10.5194/acp-15-5405-2015](https://doi.org/10.5194/acp-15-5405-2015).

Li, D., et al. (2017). How much runoff originates as snow in the western United States, and how will that change in the future? *Geophys. Res. Lett.*, 6163–6172. doi:[10.1002/2017GL073551](https://doi.org/10.1002/2017GL073551).

Lin, Y., et al. (2022), Modeling impacts of ice-nucleating particles from marine aerosols on mixed-phase orographic clouds during 2015 ACAPEX field campaign, *Atmos. Chem. Phys.*, **22**, 6749–6771. doi:[10.5194/acp-22-6749-2022](https://doi.org/10.5194/acp-22-6749-2022).

Liston, G. E., and Sturm, M. (2002). Winter precipitation patterns in arctic Alaska determined from a blowing-snow model and snow-depth observations. *J. Hydromet.*, **3**, 646–659. doi: [10.1175/1525-7541\(2002\)003<0646:WPPIAA>2.0.CO;2](https://doi.org/10.1175/1525-7541(2002)003<0646:WPPIAA>2.0.CO;2)

Loeb, N. A., & Kennedy, A. (2022). Blowing snow at McMurdo station, Antarctica during the AWARE Field Campaign: Surface and ceilometer observations. *J. Geophys. Res. Atmos.*, **126**, e2020JD033935. doi:[10.1029/2020JD033935](https://doi.org/10.1029/2020JD033935).

Lukas, J. & E. Payton, eds. (2020). *Colorado River Basin Climate and Hydrology: State of the Science. Western Water Assessment*, University of Colorado Boulder. doi: [10.25810/3hcv-w477](https://doi.org/10.25810/3hcv-w477).

Lundquist J.D., et al. (2003). Meteorology and Hydrology in Yosemite National Park: A Sensor Network Application. In: Zhao F., Guibas L. (eds) Information Processing in Sensor Networks. Lecture Notes in Computer Science, vol 2634. Springer, Berlin, Heidelberg. doi:[10.1007/3-540-36978-3\\_35](https://doi.org/10.1007/3-540-36978-3_35).

Lundquist, J.D., et al. (2015), High-Elevation Precipitation Patterns: Using Snow Measurements to Assess Daily Gridded Datasets across the Sierra Nevada, California. *J. Hydromet.*, **16**, 1773–1792, doi: [10.1175/JHM-D-15-0019.1](https://doi.org/10.1175/JHM-D-15-0019.1).

Lundquist, J., et al., (2019) Our Skill in Modeling Mountain Rain and Snow is Bypassing the Skill of Our Observational Networks, *Bull. Amer. Meteor. Soc.*, 2473-2490, doi: [10.1175/BAMS-D-19-0001.1](https://doi.org/10.1175/BAMS-D-19-0001.1).

Maddox, R.A., et al. (2002). Weather Radar Coverage over the Contiguous United States. *Wea. Forecasting*, **17**, 927–934, doi:[10.1175/1520-0434\(2002\)017<0927:WRCOTC>2.0.CO;2](https://doi.org/10.1175/1520-0434(2002)017<0927:WRCOTC>2.0.CO;2).

Maina, F.Z., et al. (2022) Projecting end-of-century climate extremes and their impacts on the hydrology of a representative California watershed, *Hydrol. Earth Syst. Sci*, **26**, 3589-3609, doi: [10.5194/hess-26-3589-2022](https://doi.org/10.5194/hess-26-3589-2022).

Mather, J. H., & Voyles, J. W. (2013). The Arm Climate Research Facility: A Review of Structure and Capabilities, *Bull. Amer. Meteor. Soc.*, **94**(3), 377-392, doi:[10.1175/BAMS-D-11-00218.1](https://doi.org/10.1175/BAMS-D-11-00218.1).

McCabe, G. J., and Wolock, D. M. (2007), Warming may create substantial water supply shortages in the Colorado River basin, *Geophys. Res. Lett.*, **34**, L22708, doi:[10.1029/2007GL031764](https://doi.org/10.1029/2007GL031764).

McCabe, G. J., and Wolock, D. M. (2009), Recent declines in western U.S. snowpack in the context of twentieth-century climate variability, *Earth Interactions*, **13**, doi:10.1175/2009EI283.1.

McCord, R., and J. Voyles, (2016) The ARM Data System and Archive. *Meteor. Monogr.*, **57**, 11.1–11.15, doi: 10.1175/AMSMONOGRAPHS-D-15-0043.1.

McFarlane, S. A., et al. (2016). ARM's Progress on Improving Atmospheric Broadband Radiative Fluxes and Heating Rates, *Meteor. Monogr.*, **57**, 20.1-20.24, doi: [10.1175/AMSMONOGRAPHS-D-15-0046.1](https://doi.org/10.1175/AMSMONOGRAPHS-D-15-0046.1).

McLaughlin, D., et al. (2009) Short-Wavelength Technology and the Potential For Distributed Networks of Small Radar Systems, *Bull. Amer. Meteor. Soc.*, **90**, 1797-1818, doi:10.1175/2009BAMS2507.1.

Miller, M. A., et al. (2016). The ARM Mobile Facilities, *Meteor. Monogr.*, **57**, 9.1-9.15, doi: [10.1175/AMSMONOGRAPHS-D-15-0051.1](https://doi.org/10.1175/AMSMONOGRAPHS-D-15-0051.1).

Milly, P.C.D., and Dunne, K.A. (2020) Colorado River flow dwindles as warming-driven loss of reflective snow energizes evaporation, *Science*, **367**(6483), 1252-1255, doi: [10.1126/science.aay9187](https://doi.org/10.1126/science.aay9187).

Mote, P.W. et al. (2018) Dramatic declines in snowpack in the western US. *npj Clim Atmos Sci* **1**, 2, doi:[10.1038/s41612-018-0012-1](https://doi.org/10.1038/s41612-018-0012-1).

Mott, R., et al. (2018). The Seasonal Snow Cover Dynamics: Review on Wind-Driven Coupling Processes, *Front. Earth Sci.*, doi:[10.3389/feart.2018.00197](https://doi.org/10.3389/feart.2018.00197).

Moulin, L., et al. (2009), Uncertainties on mean areal precipitation: assessment and impact on streamflow simulations, *Hydrol. Earth Syst. Sci.*, **13**, 99-114, doi:[10.5194/hess-13-99-2009](https://doi.org/10.5194/hess-13-99-2009).

Mühlbauer, A. and U. Lohmann (2006), Aerosol-cloud interactions and the effects on orographic precipitation. In 12th AMS Conference on Cloud Physics, Madison, USA (pp. 10-14).

Mühlbauer, A. and U. Lohmann (2008), Sensitivity studies of the role of aerosols in warm-phase orographic precipitation in different dynamical flow regimes. *J. Atmos. Sci.*, **65**(8), 2522-2542, doi:[10.1175/2007JAS2492.1](https://doi.org/10.1175/2007JAS2492.1).

Musselman, K.N. et al. (2017) Slower snowmelt in a warmer world, *Nature Clim. Change*, **7**, 214-219, doi: [10.1038/nclimate3225](https://doi.org/10.1038/nclimate3225).

Musselman, K. N., et al. (2018), Projected increases and shifts in rain-on-snow flood risk over western North America. *Nature Clim. Change*, **8**, 808-812, doi:[10.1038/s41558-018-0236-4](https://doi.org/10.1038/s41558-018-0236-4).

National Research Council, Board on Atmospheric Sciences and Climate, *Weather radar technology beyond NEXRAD*, National Academies Press, Washington, 2002, pp. 81.

Neelin, J. D. (2007). *Moist dynamics of tropical convection zones in monsoons, teleconnections, and global warming*. In T. Schneider & A. H. Sobel (Eds.), *The Global Circulation of the Atmosphere* (pp. 267–301). Princeton, NJ: Princeton University Press.

NRCS, (2022) SNOWpack TELEmetry Network (SNOTEL).. <https://data.nal.usda.gov/dataset/snowpack-telemetry-network-snotel> for Butte (380) station. Accessed 2022-12-01.

Painter, T., et al. (2007) Contact spectroscopy for determination of stratigraphy of snow optical grain size. *Journal of Glaciology*, **53**(180), 121-127.

doi:[10.3189/172756507781833947](https://doi.org/10.3189/172756507781833947).

Painter, T., et al. (2009) Retrieval of subpixel snow covered area, grain size, and albedo from MODIS, *Remote Sens. Environ.*, **113**(4), 868-879, doi: [10.1016/j.rse.2009.01.001](https://doi.org/10.1016/j.rse.2009.01.001).

Painter, T. H., Bryant, A. C., and Skiles, S. M. (2012), Radiative forcing by light absorbing impurities in snow from MODIS surface reflectance data, *Geophys. Res. Lett.*, **39**, L17502, doi: [10.1029/2012GL052457](https://doi.org/10.1029/2012GL052457).

Painter, T. H., et al (2016) The Airborne Snow Observatory: Fusion of scanning lidar, imaging spectrometer, and physically-based modeling for mapping snow water equivalent and snow albedo, *Remote Sens. Environ.*, **184**, 139-152, doi: [10.1016/j.rse.2016.06.018](https://doi.org/10.1016/j.rse.2016.06.018).

Ramanathan, V. and G. Carmichael (2008). Global and regional climate changes due to black carbon. *Nat. Geosci.*, **1**, 221–227, doi:[10.1038/ngeo156](https://doi.org/10.1038/ngeo156).

Pan, M., et al. (2003). Snow process modeling in the North American Land Data Assimilation System (NLDAS): 2. Evaluation of model simulated snow water equivalent. *J. Geophys. Res.*, **108**, 8850. doi:[10.1029/2003JD003994](https://doi.org/10.1029/2003JD003994).

Peppler, R. A., K. E. Kehoe, J. W. Monroe, A. K. Theisen, and S. T. Moore, (2016) The ARM Data Quality Program. *Meteor. Monogr.*, **57**, 12.1–12.14, doi:10.1175/AMSMONOGRAPHS-D-15-0039.1.

Rasmussen, R., et al (2012), How well are we measuring snow: The NOAA/FAA/NCAR winter precipitation test bed. *Bull. Amer. Meteor. Soc.*, **93**, 811–829, doi:[10.1175/BAMS-D-11-00052.1](https://doi.org/10.1175/BAMS-D-11-00052.1).

Rhoades, A. M., et al. (2018a). Projecting 21st century snowpack trends in western USA mountains using variable-resolution CESM, *Clim. Dyn.*, **50**, 261-268, doi:[10.1007/s00382-017-3606-0](https://doi.org/10.1007/s00382-017-3606-0).

Rhoades, A. M., et al. (2018b). Sensitivity of mountain hydroclimate simulations in variable-resolution CESM to microphysics and horizontal resolution. *J. Adv. Model. Earth Syst.*, **10**, 1357– 1380. doi:[10.1029/2018MS001326](https://doi.org/10.1029/2018MS001326).

Rittger, K., et al. (2021) Multi-sensor fusion using random forests for daily fractional snow cover at 30 m, *Remote Sens. Environ.*, **264**, doi: [10.1016/j.rse.2021.112608](https://doi.org/10.1016/j.rse.2021.112608).

Rudisill, W., et al. (2022) *Dynamically Downscaled (WRF) 1km, Hourly Meteorological Conditions 1987-2020. East/Taylor Watersheds*. United States: N. p., doi:[10.15485/1845448](https://doi.org/10.15485/1845448).

Ryken, A. C., et al. (2022). Unravelling groundwater contributions to evapotranspiration and constraining water fluxes in a high-elevation catchment. *Hydrol. Process.*, **36**(1), e14449. <https://doi.org/10.1002/hyp.14449>

Saleeby, S.M., et al. (2011), The cumulative impact of cloud droplet nucleating aerosols on orographic snowfall in Colorado. *J. Appl. Meteorol. Climatol.*, **50**(3), 604-625, doi:[10.1175/2010JAMC2594.1](https://doi.org/10.1175/2010JAMC2594.1).

Santos, N. (2021) Operation Plan for Colorado River System Reservoirs 24-month plan, <https://www.usbr.gov/lc/region/g4000/24mo.pdf>.

Serreze, M. C., et al. (1999), Characteristics of the western United States snowpack from snowpack telemetry (SNOTEL) data, *Water Resour. Res.*, **35**(7), 2145– 2160, doi:[10.1029/1999WR900090](https://doi.org/10.1029/1999WR900090).

Sevruk, B. (1997). Regional Dependency of Precipitation-Altitude Relationship in the Swiss Alps. *Clim. Change*, **36**, 355, doi:[10.1023/A:1005302626066](https://doi.org/10.1023/A:1005302626066).

Sexstone, G. A., et al. (2016) Comparison of methods for quantifying surface sublimation over seasonally snow-covered terrain. *Hydrol. Process.*, **30**: 3373– 3389.  
doi: [10.1002/hyp.10864](https://doi.org/10.1002/hyp.10864).

Skiles, S. M., et al. (2015) Regional variability in dust-on-snow processes and impacts in the Upper Colorado River Basin. *Hydrol. Process.*, **29**, 5397–5413. doi: [10.1002/hyp.10569](https://doi.org/10.1002/hyp.10569).

Skiles, S.M., and T.H. Painter (2016) A 9-yr record of dust-on-snow in the Colorado River Basin, Proceedings of the 12th Biennial Conference of Science and Management on the Colorado Plateau, *U.S. Geological Survey Scientific Investigations Report 2015–5180*, 3-11, doi: [10.3133/sir20155180](https://doi.org/10.3133/sir20155180).

Skiles, S.M., and T.H. Painter (2017) Daily evolution in dust and black carbon content, snow grain size, and snow albedo during snowmelt, Rocky Mountains, Colorado, *J. Glaciol.*, **63** (237), 118-132. doi: [10.1017/jog.2016.125](https://doi.org/10.1017/jog.2016.125).

Stoelinga, M. T., et al. (2013), Microphysical processes within winter orographic cloud and precipitation systems, in *Mountain Weather Research and Forecasting*, edited by F. Chow et al., pp. 345–408, Springer Atmospheric Sciences, doi: [10.1007/978-94-007-4098-3\\_7](https://doi.org/10.1007/978-94-007-4098-3_7).

Svoma, B.H., (2016) Difficulties in Determining Snowpack Sublimation in Complex Terrain at the Macroscale, *Adv. Meteor.*, doi:10.1155/2016/9695757.

UCAR/NCAR - Earth Observing Laboratory. (1990). NCAR Integrated Surface Flux System (ISFS). UCAR/NCAR - Earth Observing Laboratory. <https://doi.org/10.5065/D6ZC80XJ>  
Retrieved February 17, 2017

Uin, J., et al. (2019). Atmospheric Radiation Measurement (ARM) Aerosol Observing Systems (AOS) for Surface-Based In Situ Atmospheric Aerosol and Trace Gas Measurements, *J. Atmos. Ocean Technol.*, **36**(12), 2429-2447, doi:[10.1175/JTECH-D-19-0077.1](https://doi.org/10.1175/JTECH-D-19-0077.1).

U.S. DOE. 2019. Atmospheric Radiation Measurement (ARM) User Facility ARM Mobile Facility Workshop Report, DOE/SC-0197 Office of Biological and Environmental Research, U.S. Department of Energy Office of Science, Germantown, Maryland, USA.  
[https://science.osti.gov/-/media/ber/pdf/community-resources/2019/ARM\\_Mobile\\_Facility\\_Workshop\\_Report.pdf](https://science.osti.gov/-/media/ber/pdf/community-resources/2019/ARM_Mobile_Facility_Workshop_Report.pdf)

U.S. DOE. 2022. Understanding and Predictability of Integrated Mountain Hydroclimate Draft Workshop Report, Office of Biological and Environmental Research, U.S. Department of Energy Office of Science, Germantown, Maryland, USA.  
[https://ess.science.energy.gov/wp-content/uploads/2022/12/Integrated\\_Mountain\\_Hydroclimate\\_report\\_Dec2022\\_DRAFT.pdf](https://ess.science.energy.gov/wp-content/uploads/2022/12/Integrated_Mountain_Hydroclimate_report_Dec2022_DRAFT.pdf)

Vano, J. A., et al. (2014). Understanding Uncertainties in Future Colorado River Streamflow, *Bull. Amer. Meteor. Soc.*, **95**(1), 59-78, doi:[10.1175/BAMS-D-12-00228.1](https://doi.org/10.1175/BAMS-D-12-00228.1).

Viviroli, D., et al. (2011), Climate change and mountain water resources: overview and recommendations for research, management and policy, *Hydrol. Earth Syst. Sci.*, **15**, 471-504, doi:[10.5194/hess-15-471-2011](https://doi.org/10.5194/hess-15-471-2011).

Williams, A. P., et al (2022), Rapid intensification of the emerging southwestern North American megadrought in 2020–2021, *Nature Clim. Change*, **12**, 232–234, doi:  
[10.1038/s41558-022-01290-z](https://doi.org/10.1038/s41558-022-01290-z).

Wolfe, J. P., and J. R. Snider, (2012) A relationship between reflectivity and snow rate for a high-altitude S-band radar. *J. Appl. Meteorol. Climatol.*, **51**, 1111–1128, doi:[10.1175/JAMC-D-11-0112.1](https://doi.org/10.1175/JAMC-D-11-0112.1).

Wu, G.-M., et al. (2016) Brown carbon in the cryosphere: Current knowledge and perspective, *Adv. Clim. Change Res.*, **7**(1-2), 82-89, doi:[10.1016/j.accre.2016.06.002](https://doi.org/10.1016/j.accre.2016.06.002).

Xiao, M., et al. (2018). On the causes of declining Colorado River streamflows. *Water Resour. Res.*, **54**, 6739– 6756, doi: [10.1029/2018WR023153](https://doi.org/10.1029/2018WR023153).

Xu, Z., et al. (2023) Sensitivities of subgrid-scale physics schemes, meteorological forcing, and topographic radiation in atmosphere-through-bedrock integrated process models: A case study in the Upper Colorado River Basin, *EGUsphere*, doi:[10.5194/egusphere-2022-437](https://doi.org/10.5194/egusphere-2022-437).

Yang, Y ., et al (2016), Mechanisms Contributing to Suppressed Precipitation in Mt. Hua of Central China, Part I -Mountain Valley Circulation, *J. Atmos. Sci.*, **73**(3):1351-1366. doi:[10.1175/JAS-D-15-0233.1](https://doi.org/10.1175/JAS-D-15-0233.1).

Zhang, Z., et al (2017), Insights into mountain precipitation and snowpack from a basin-scale wireless-sensor network, *Water Resour. Res.*, **53**, 6626–6641, doi:[10.1002/2016WR018825](https://doi.org/10.1002/2016WR018825).